ARTICLE INFO
Article ID: 04-13-01-0003

doi:10.4271/04-13-01-0003

A Modeling Study of an Advanced Ultra-low NO_x Aftertreatment System

Venkata Rajesh Chundru,[1] John H. Johnson,[1] and Gordon G. Parker[1]

[1]Michigan Technological University, USA

Abstract

The 2010 Environmental Protection Agency (EPA) Emission Standard for heavy-duty engines required 0.2 g/bhp-hr over certification cycles (cold and hot Federal Test Procedure [FTP]), and the California Air Resources Board (CARB) standards require upto 90% reduction of overall oxides of nitrogen (NOx) emissions. Similar reductions may be considered by the EPA through its Cleaner Trucks Initiative program. In this article, aftertreatment system components consisting of a diesel oxidation catalyst (DOC); a selective catalytic reduction catalyst on a diesel particulate filter (DPF), or SCR-F; a second DOC (DOC_2); and a SCR along with two urea injectors have been analyzed, which could be part of an aftertreatment system that can achieve the 0.02 g/bhp-hr standard. The system performance was evaluated using validated one-dimensional (1D) DOC, two-dimensional (2D) SCR-F, and 1D SCR models at various combinations of inlet ammonia (NH_3)-to-NO_x ratio (ANR) values for the SCR-F and the SCR to determine the injection rates required to achieve an optimum nitrogen dioxide (NO_2)/NO_x ratio at the inlets of both the SCR-F and the SCR. A strategy was developed that yielded 99.5% NO_x conversion at inlet temperatures from 203° to 450°C, while maximizing particulate matter (PM) oxidation rate in the SCR-F and minimizing the urea consumption rate. These system components have the potential to be robust to variations in the inlet NO_x and NH_3 concentrations and the NO_x conversion performance of the system components.

NO_x conversions greater than 95% in the SCR-F and SCR were determined to be primarily due to the fast SCR reaction. The two urea injectors were used to maximize NO_x reduction in both devices and SCR-F PM oxidation. For the case with ANR_1 = 0, a 90%-100% increase in NO_2-assisted PM oxidation in the SCR-F was determined compared to a system without the second DOC and urea injector. Further development of the system components should be pursued in terms of catalyst type, catalyst loading, and external heating along with a close-coupled SCR/DOC or passive NO_x adsorbers (PNA) to reduce the light-off time for cold-start emissions control.

History

Received: 21 Jun 2019
Revised: 08 Oct 2019
Accepted: 03 Dec 2019
e-Available: 09 Jan 2020

Keywords

SCR-F, Ultra low NOx, Aftertreatment, CPF, SCR, DOC, PNA, Design, Modeling, Catalyst

Citation

Chundru, V., Johnson, J., and Parker, G., "A Modeling Study of an Advanced Ultra-low NO_x Aftertreatment System," *SAE Int. J. Fuels Lubr.* 13(1):37–60, 2020, doi:10.4271/04-13-01-0003.

ISSN: 1946-3952
e-ISSN: 1946-3960

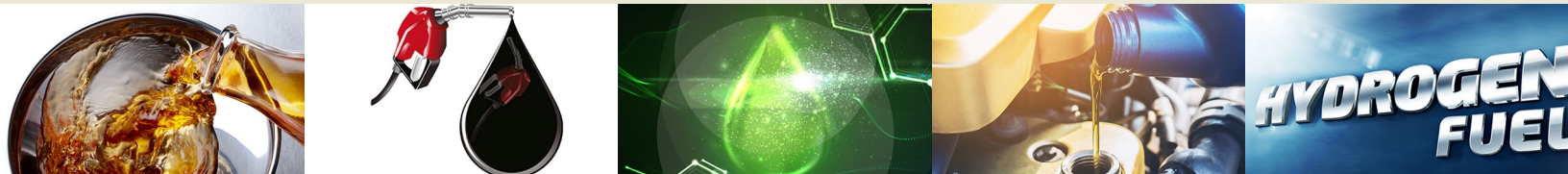

Introduction

The ultra-low NO_x standard of 0.02 g/bhp-hr has been proposed by CARB. The EPA will publish in 2020 a proposed rule to further reduce NOx as part of the Cleaner Trucks Initiative [1]. Validated models consisting of a 1D DOC [2], a 2D SCR-F [3], and a 1D SCR [4] were used to simulate the aftertreatment system components in this article to simulate a system that can achieve this NO_x standard.

In order to meet the ultra-low NO_x standards of 0.02 g/bhp-hr, a system that can achieve greater than 99.5% NO_x conversion for both cold and hot parts of the cycle is required. New aftertreatment system components consisting of a DOC, urea injector + decomposition tube, SCR-F, DOC_2, urea injector 2 + decomposition tube 2, and SCR (Patent Pending) are able to meet the emissions performance characteristics for typical engine operating conditions with the potential to meet the standards utilizing a system with a diesel cold-start catalyst (dCSC™) in place of the first DOC. The system components primarily increase the performance of the downstream SCR by optimizing the SCR inlet NO_2/NO_x ratio using the NO oxidation reaction in the second DOC. This optimum NO_2/NO_x ratio in the range of 0.4-0.5 promotes a fast SCR reaction in the SCR, thus leading to >99.5% NO_x conversion efficiency. The resultant system with a SCR-F and SCR NO_x conversion efficiencies of 97.5% and 95% leads to system NO_x conversion of greater than 99.5%. This aspect of the system was developed based on previous work by the authors described in reference [5], where the performance of the downstream SCR in a SCR-F + SCR system with one injector was found to be severely limited due to the near-zero NO_2/NO_x ratio at the SCR inlet.

This research focuses on determining the performance characteristics of the system and comparing it with existing SCR-F systems using system-level models consisting of a combination of 2D SCR-F, 1D DOC, and 1D SCR models. These models have been calibrated using experimental data collected on a Cummins 2013 interact series B (ISB) and a Cummins 2010 ISB engine from references [6, 7, 8].

The major objectives of this article are

1. Model engine operating conditions for components in a new aftertreatment system consisting of a DOC, urea injector 1, SCR-F, DOC_2, urea injector 2, and SCR and for high NO_x conversion and increased PM oxidation rate compared to other SCR-F systems.
2. Conduct a parametric study that describes the performance characteristics of the DOC/SCR-F/DOC_2 and SCR system and compare it with other systems in terms of NO_x conversion, PM oxidation, and urea consumption performance.
3. Describe the control strategy that can be used to effectively use the system performance characteristics with the DOC/SCR-F/DOC_2 and SCR components to optimize the NO_x conversion efficiency and the PM oxidation rate.

This article is divided into seven sections. The Literature Review summarizes recent advances in SCR-F modeling from the open literature which plays an important role in the design of the various ultra-low NO_x aftertreatment system architectures. This is followed by a description of ultra-low NO_x aftertreatment systems and SCR-F patents which form the underlying technologies for the proposed system. The literature review is followed by a description of the aftertreatment component models and experimental data section consisting of the specifications of the aftertreatment system components used in the modeling effort.

The modeled aftertreatment system section looks at various existing and proposed system architectures including the advantages and disadvantages of each system. This section also describes system-level model architecture of the system modeled.

The results section consists of a parametric study used to study and analyze the NO_x reduction and PM oxidation performance of both the existing and proposed ultra-low NO_x system. The control system design for the ultra-low NO_x system is also described in this section along with possible control algorithms that can be used to optimize the performance of the DOC + SCR-F + DOC_2 + SCR system components. The Summary/Conclusions section deals with the major conclusions and future work with respect to the ultra-low NO_x system components in terms of catalyst development, external heat for cold start, and sizing of the components.

Literature Review

Since the SCR-F is used in all four of the aftertreatment systems analyzed later, recent advances in its use and modeling are considered first. This is followed by a review of ultra-low NO_x aftertreatment system studies.

SCR-F Modeling

In SCR-F modeling, the interaction of the SCR reactions and the NO_2-assisted PM oxidation reactions leading to competition for NO_2 are an important chemical phenomenon along with PM filtration phenomena that needs to be accurately modeled. These phenomena play an important role in determining the NO_x conversion and PM oxidation performance of the SCR-F and the NO_x conversion performance of the downstream SCR [5, 9] which are used in typical systems being considered for ultra-low NO_x applications.

The interaction of different reactions in the substrate wall and PM cake is modeled using a reaction diffusion scheme used in reference [3]. Accurate simulation of the internal states are achieved by simulating the forward diffusion of NO_2 from PM cake to the wall, the inhibition of SCR reactions due to mass transfer limitation caused by PM deposited in the substrate wall, and the change in the local NO_2/NO_x ratio in the PM cake and different wall layers. Park et al. [10, 11]

developed a 1D model capable of simulating inhibition of the SCR reactions due to mass transfer limitations by wall PM, and change in local NO_2/NO_x ratio across the PM cake layer. Yang et al. [12] also found similar inhibitions of the SCR reactions due to wall PM while Colombo et al. [13] developed a model that accurately simulates the change in the NO_2/NO_x ratio across the SCR-F.

Determining the number of active sites for NH_3 storage and modeling the number of active catalytic sites is an important criterion for modeling the SCR reaction rates and NH_3 slip in a SCR-F. Modeling of the catalyst sites permits simulating the deterioration of the SCR-F due to aging, sulfur poisoning, and ash accumulation, all of which are important for real-world compliance in ultra-low NO_x systems. Lopez et al. [14] modeled a vanadium-based catalyst where the number of active sites was proportional to catalyst loading inside the substrate wall. Similarly, Dosda et al. [15] modeled copper-zeolite (Cu-Ze) catalyst deterioration due to thermal gaining caused by cupric oxide (CuO) accumulation in the catalyst sites, and Tan et al. [16] developed a model that showed a 30% reduction in NH_3 storage due to PM loading in the wall. Tronoconi et al. [17] developed a two-site storage model in Axisuite® for a SCR-F to simulate NH_3 slip and forward diffusion of NO_2 between the PM cake and the substrate wall layer to quantify the impact of the SCR reactions on the PM oxidation rate. This model also simulates pressure drop and filtration characteristics of the SCR-F.

Ultra-low NOx Systems

Based on the SCR-F modeling studies, the NO_x conversion efficiency of present-day SCR-Fs is low at inlet temperatures less than 250°C and is further impacted by thermal aging, ash loading, inhibition due to PM loading in the wall, sulfur, poisoning unfavorable NO_2/NO_x ratio at the SCR-F inlet, and consumption of NO_2 by the PM oxidation reaction in the PM cake. In order to overcome these limitations and achieve the ultra-low NO_x, standard a system capable of >99.5% NO_x conversion is required for both cold and hot parts of the test cycle. Different combinations of SCR-F, SCR, DOC, and PNA are being proposed in the literature to meet this requirement.

Sharp et al. [18, 19, 20] studied different configurations of aftertreatment systems that have the potential to meet the ultra low NO_x CARB standard for both cold start conditions and the hot part of the cycle. A system consisting of PNA + Mini Burner (MB) + SCR-F + SCR + ammonia slip catalyst (ASC) was found to achieve the required goal. The engine calibration in terms of EGR during cold-start conditions was changed to obtain faster catalyst light-off time for the SCR-F and SCR, and external heat was added to the system using the MB upstream of the SCR-F. For the test cycle consisting of 1/7th cold-start conditions and 6/7th hot part of the cycle, a combined NO_x conversion efficiency of 99.4% was found to be the target system performance to meet the ultra-low NO_x standard. It was concluded that a combination of the addition of external heat and engine calibration is required to achieve ultra-low NO_x emissions.

Strots et al. [21] developed a system model consisting of a 1D SCR-F and 1D SCR model to simulate the NO_x reduction performance. Experimental data were collected on a six-cylinder 255 KW Euro 5 engine with the World Harmonized Transient Cycle (WHTC) cycle. A DOC + DPF + SCR + ammonia oxidation catalyst (AMOX) system was compared to a DOC + SCR-F + SCR + AMOX system. The SCR-F was found to have faster light off compared to the DPF + SCR system due to lower system thermal mass. A lower operating temperature by about 8°C for the SCR was observed compared to the SCR-F, leading to higher NO_x conversion performance of the SCR-F-based system. Further studies on the change in NO_2 concentration caused by the reaction diffusion scheme in the SCR-F due to the fast SCR reaction are needed.

Georgiadis et al. [22] designed a system to reduce the nonuniformity of NH_3 at the SCR-F inlet. Using this system, accurate control of NH_3 coverage fraction in the SCR-F is possible in real-world operation eliminating the need for the AMOX downstream of the SCR.

Hurby et al. [23] found significant decrease in NO_x conversion performance of a SCR-F downstream of a DOC. This drop in SCR-F NO_x conversion was found to be a function of platinum group metal (PGM) transport from the DOC channel surface to the PM cake layer of the SCR-F, leading to excess NH_3 oxidation. This phenomenon could have a major impact on SCR-F-based ultra-low NO_x systems in real-world conditions. PGM transport phenomena from the DOC need to be further studied, and measures to mitigate this phenomenon need to be developed to ensure long-term reliability of SCR-F-based ultra-low NO_x systems.

CARB is doing R&D to develop an optimal prototype system with a close-coupled SCR along with DOC, SCR-F, and SCR. This stage 1 system primarily focuses on improving the cold-start performance of the system by the addition of close-coupled SCR at turbo out and addition of external heat using MBs and electrical heaters. The downstream SCR in a SCR-F + SCR system is limited in terms of its role in NO_x conversion performance due to unfavorable inlet NO_2/NO_x ratio as described in reference [5].

Recently, several aftertreatment configurations to meet the levels expected for the 2024 CARB ultra-low NO_x standards and EPA 2027 standards were proposed at the University of Wisconsin Madison Symposium. Presentations at this symposium on ultra-low NO_x systems by EPA [25] and CARB [26] highlighted the importance of advanced aftertreatment systems for low-load cycles, real-world compliance and lower NO_x emissions as part of the Cleaner Trucks Initiative. Different advanced aftertreatment systems were presented by CARB with different combinations of DOC, SCR-F, SCR, and ASC shown in Figure 1 that can potentially meet the ultra-low NO_x standards.

Cummins Emissions Solution presented a possible ultra-low NO_x configuration component based on a single-pump dual-injector system for a SCR-F and SCR-based system along with close-coupled SCR [27, 28]. Southwest Research Institute (SwRI) [29] presented an update on the CARB sponsored program that utilizes systems similar to those shown in Figure 1 to meet the ultra low NO_x standard.

FIGURE 1 Advanced aftertreatment being considered by CARB for ultra low NOx standard [26] for stage 3 research (Reprinted from [26]. California Air Resources Board).

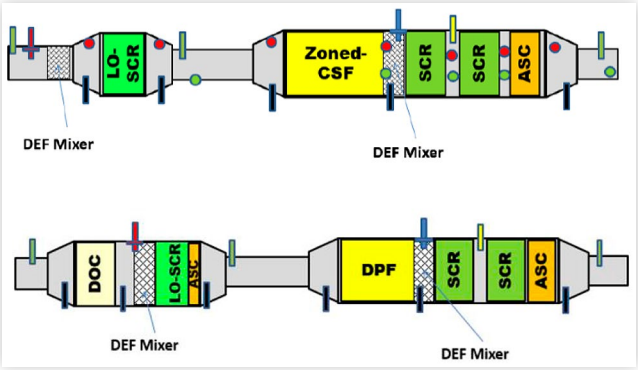

Several possible aftertreatment configurations have been proposed recently to meet the ultra-low NO_x standard [24, 25, 26, 27, 28, 29]. The major trends observed in all these systems consist of close-coupled SCR systems, addition of external heating, tuning of engine calibration for cold-start conditions, and replacing the DOC with a PNA. Dual-injection systems for SCR-F with downstream SCR are also being proposed.

The major factors that limit the performance of a SCR-F in terms of NO_x reduction are catalyst aging, ash loading, and transport of the PGM from upstream DOC [23]. All of these factors lead to significant reduction of the NO_x conversion of the SCR-F in real-world conditions combined with unfavorable NO_2/NO_x ratio at the SCR inlet. The research in this article focuses on improving the performance of the downstream SCR and at the same time leverage the added flexibility of two injectors in terms of ensuring high system NO_x conversion for conditions where the SCR-F performance is reduced by the abovementioned factors using a suitable control strategy for the two urea injectors. Further increase in the SCR-F PM oxidation rate is also achieved by reducing the forward diffusion of NO_2 using the two injectors. Some of the work on the SCR-F and the underlying technologies are based on patents by BASF from references [30, 31, 32, 33, 34, 35, 36, 37, 38, 39]. The research in this article focuses on modeling the SCR-F + SCR system with the addition of a DOC_2 between the SCR-F and SCR to increase the downstream SCR performance with a focus on the hot part of the cycle. Such a system can be incorporated as part of the mentioned aftertreatment systems above to meet the overall cycle ultra low NO_x requirements consisting of both cold-start and hot conditions.

Model Description and Experimental Data

In order to evaluate the performance of the systems studied in this research, 2D SCR-F [3], 1D DOC [2], and 1D SCR [4] models were used. These models were validated using engine experimental data as described in references [1, 6, 7, 8]. The development of the 2D SCR-F model used in the simulations was started based on the literature review by Xiaobo Song et al. [9]. Based on this review, the important features of the SCR-F model including the forward diffusion of NO_2, low-temperature performance and catalyst placement, and competition for NO_2 between PM oxidation and SCR reactions were included in the 2D SCR-F model. A set of experiments were conducted using the DOC + SCR-F + SCR system using a 2013 6.7 L Cummins ISB engine described in reference [6] and were modeled using the SCR-F model [3] and the SCR model [4]. Similarly, a set of experiments were performed as described in reference [7] with the aftertreatment system consisting of a DOC + SCR-F with and without urea injection.

A system model consisting of a 2D SCR-F, 1D DOC, and 1D SCR models has been used to model the various systems. The 2D SCR-F model described in reference [3] is capable of simulating the exhaust gas outlet temperature, PM oxidation, SCR reactions, PM mass retained, and pressure drop characteristics of the SCR-F. The outlet concentrations of NO, NO_2, and NH_3 from the SCR-F model were used as the input to simulate the downstream components. The kinetics for the DOC model is based on the 2010 ISB engine data from reference [2]. The 1D SCR model described in reference [4] was used to model downstream emissions from the SCR-F model for a SCR-F + SCR system. A brief description of these models is given in this section.

2D SCR-F Model

The 2D SCR-F model can simulate the internal states of 2D temperature, PM mass retained, and NH_3 coverage fraction distributions. The PM oxidation and SCR reaction kinetics in the model were calibrated using data from a Johnson Matthey SCRF® with a Cummins 6.7 L 2013 ISB engine. A two-site model, with the first site participating in SCR reactions and storage and the second site participates only in storage, has been used. A reaction diffusion scheme has been used to simulate the change in NO, NO_2, and NH_3 concentrations due to the SCR and PM oxidation reactions across the PM cake and substrate wall layers. Forward diffusion of NO_2 between the PM cake and substrate wall layers and the resultant 70% reduction in NO_2-assisted PM oxidation rate due to SCR reactions are modeled. The inhibition in SCR reactions due to the decrease in mass transfer caused by PM in the substrate wall is also taken into account. The list of reactions in this model is shown in Table 1 with * representing the adsorbed NH_3 on the catalyst sites. Equations 1-5 represent the governing equations for species conservation in the inlet/outlet channels, substrate wall, and NH3 storage on the two storage sites.

$$\frac{dC_{1,l}}{dt} = -v_1 \frac{dC_{1,l}}{dx} + \left(\frac{4}{a}\right) k_1 \left(C_{1s,l} - C_{1,l}\right) + \left(\frac{4}{a}\right) v_f C_{1,l} \quad \text{Eq. (1)}$$

TABLE 1 2D SCR-F model reactions.

Reaction name	Reaction
NH_3 adsorption/ desorption at sites 1 and 2	$NH_3 \leftrightarrow NH_3^*$
Fast SCR	$NH_3^* + \frac{1}{2}NO + \frac{1}{2}NO_2 \rightarrow N_2 + \frac{3}{2}H_2O$
Slow SCR	$NH_3^* + \frac{3}{4}NO_2 \rightarrow \frac{7}{8}N_2 + \frac{3}{2}H_2O$
Standard SCR	$NH_3^* + NO + \frac{1}{4}O_2 \rightarrow N_2 + \frac{3}{2}H_2O$
NH_3 oxidation	$NH_3^* + \frac{3}{4}O_2 \rightarrow \frac{1}{2}N_2 + \frac{3}{2}H_2O$
NO oxidation	$NO + \frac{1}{2}O_2 \rightarrow NO_2$
Passive PM oxidation	$C + (2 - g_{CO})NO_2 \rightarrow g_{CO}\ CO + (1 - g_{CO})\ CO_2 + (2 - g_{CO})NO$
Thermal PM oxidation	$C + \left(1 - \frac{f_{CO}}{2}\right)O_2 \rightarrow f_{CO}\ CO + (1 - f_{CO})CO_2$
CO oxidation	$CO + \frac{1}{2}O_2 \rightarrow CO_2$
HC oxidation	$C_{12}H_{24} + 18\ O_2 \rightarrow 12\ CO_2 + 12\ H_2O$

* Adsorbed NH_3 on catalytic site

$$\frac{dC_{f,l}}{dt} = -v_f \frac{dC_{f,l}}{dy} + \frac{d}{dy}\left(D_l \frac{dC_{f,l}}{dy}\right) - \sum\nolimits_k \xi_{l,m} R_m \quad \text{Eq. (2)}$$

$$\frac{dC_{2,l}}{dt} = -v_2 \frac{dC_{2,l}}{dx} + \left(\frac{4}{a}\right)k_2\left(C_{2,l} - C_{2s,l}\right) + \left(\frac{4}{a}\right)v_f C_{2s,l} \quad \text{Eq. (3)}$$

$$\frac{d\theta_1}{dt} = \frac{\left(R_{ads,1} - R_{des,1} - 4R_{std} - 4R_{fst} - 4R_{slo} - 4R_{oxid}\right)}{\Omega_1} \quad \text{Eq. (4)}$$

$$\frac{d\theta_2}{dt} = \frac{\left(R_{ads,2} - R_{des,2}\right)}{\Omega_2} \quad \text{Eq. (5)}$$

Equation 2 is responsible for simulating the change in chemical species across the PM cake and wall layers through mass transfer by convection, diffusion, and consumption of species by the SCR and PM oxidation reactions. Equations 1 and 3 model the mass transfer in the inlet and outlet channels and are coupled with Equation 2 through mass transfer terms. The change in coverage fraction of the two sites is tracked by Equations 4 and 5. The catalytic coating was assumed to be deposited inside the substrate wall.

Energy conservation equations in 2D are used to compute the 2D temperature distribution of the exhaust gas in the inlet/outlet channels and substrate wall using Equations 6 to 8. These equations are coupled with Equations 1 to 5 using the chemical reactions energy release terms, which are part of Equation 7.

$$\rho_g C_v V_1 \frac{dT_1}{dt} = \dot{m}_{1,in} c_p \left(T_{1,i-1} - T_{1,i}\right) - \dot{m}_f c_p \left(T_{1,i-1} - T_{1,i}\right) + \dot{Q}_1 \quad \text{Eq. (6)}$$

$$\left(\rho_c C_c V_c + \rho_w C_w V_w\right)\frac{dT_f}{dt} = \dot{m}_f c_p \left(T_{1,i-1} - T_{f,i}\right) + \dot{Q}_f \quad \text{Eq. (7)}$$

$$\rho_g C_v V_2 \frac{dT_2}{dt} = \dot{m}_{2,in} c_p \left(T_{2,i-1} - T_{2,i}\right) + \dot{m}_f c_p \left(T_{f,i} + T_{2,i}\right) + \dot{Q}_2 \quad \text{Eq. (8)}$$

The SCR-F model takes into account the change in local NO_2/NO_x concentration in the substrate wall due to the consumption of NO_2 by the NO_2-assisted PM oxidation reaction. This phenomenon has a significant impact on NO_x conversion in the SCR-F and on the inlet NO_2/NO_x ratio for the downstream SCR in ultra-low NO_x systems.

The pressure drop in the SCR-F model is computed by Darcy's equation and friction factor in the inlet and outlet channels, wall, and PM cake layers. The total pressure drop across the device is computed using Equation 9:

$$\Delta P_i = P_1\big|_{x=0} - P_2\big|_{x=Li} = \Delta P_{cake} + \Delta P_{wall} + \Delta P_{channel} \quad \text{Eq. (9)}$$

where ΔP_{cake}, ΔP_{wall}, and $\Delta P_{channel}$ are the pressure drop across PM cake, wall layers, and inlet and outlet channels. The pressure drop in the PM cake and wall layers increases with increase in PM deposition and is computed by Equations 10 and 11.

$$\Delta P_{wall} = \mu v_w \frac{w_s}{k_{wall}} \quad \text{Eq. (10)}$$

$$\Delta P_{cake} = \mu v_s \frac{w_p}{k_{cake}} \quad \text{Eq. (11)}$$

The pressure drop from Equation 9 represents a single streamline. The average of pressure drop across all streamlines in the given cell is used to compute the pressure drop. Based on the pressure drop obtained, the mass flow rate profile at the inlet of the SCR-F inlet is computed in an iterative solution shown in Equation 12. A detailed explanation of these equations is given in reference [3].

$$\Delta P_{SCR-F} = \frac{\dot{m}_{total}}{\sum_{i=1}^{M} \frac{\dot{m}_i}{\Delta P_{SCR-F,i}}} \quad \text{Eq. (12)}$$

The filtration of PM in the PM cake and wall layers is computed using a unit collector concept from reference [5]. The wall layer is divided into four slabs to track PM as it passes

through thee PM cake and wall layers. Equation 13 is used to compute the total filtration efficiency

$$\eta_{total} = 1 - \left[\left(1 - \eta_{cake}\right) \prod_{n=1}^{P} \left(1 - \eta_{wall_n}\right) \right] \quad \text{Eq. (13)}$$

PM oxidation rate is computed in the PM cake and wall layers by taking both O_2-based and NO_2-assisted PM oxidation rate into account. This oxidation rate is combined with PM filtration model to track the change in PM mass retained in the PM cake and wall layers over time. Equations 14 and 15 are used to compute PM oxidation rate in the PM cake and wall layers

$$\dot{m}_{c,oxid} = \frac{s_p C_{O_2} k_{O_2} W_c}{\alpha_{o_2} \rho_s} m_c - \frac{s_p C_{NO_2} k_{NO_2} W_c}{\alpha_{NO_2} \rho_s} m_c \quad \text{Eq. (14)}$$

$$\dot{m}_{w,oxid} = \frac{s_p C_{O_2} k_{O_2} W_w}{\alpha_{o_2} \rho_w} m_w - \frac{s_p C_{NO_2} k_{NO_2} W_w}{\alpha_{NO_2} \rho_w} m_w \quad \text{Eq. (15)}$$

The model simulates pressure drop and the filtration characteristics of the SCR-F. The model was able to simulate exhaust gas temperature to within ±5°C, pressure to within ±0.1 kPa, PM mass retained to ±2 g, and outlet NO, NO_2, and NH_3 concentrations to within ±20 ppm for the 20 steady-state engine conditions used for calibration and validation, making it suitable for system simulations.

1D SCR Model

A 1D SCR model was used to simulate the NOx conversion performance of the downstream SCR in the system. This model employs a two-site storage model with SCR reactions from Table 1. A detailed description of the model is given in reference [4]. Experimental `data in the temperature range of 200-450°C from reference [6] was used to calibrate the kinetics. The resultant model based on species conservation equations in Equations 16 to 19 is capable of simulating the outlet NO, NO_2, and NH_3 concentrations to within ±20 ppm of experimental values.

$$\epsilon \frac{\partial C^n_{g,i}}{\partial t} = -u \frac{\partial C^n_{g,i}}{\partial x} - \beta_i A_g \left(C^n_{g,i} - C^n_{s,i} \right) \quad \text{Eq. (16)}$$

$$\left(1 - \epsilon\right) \frac{\partial C^n_{s,i}}{\partial t} = \beta_i A_g \left(C^n_{g,i} - C^n_{s,i} \right) - \sum\nolimits_j N_{i,j} R_j \quad \text{Eq. (17)}$$

$i = \mathrm{NO}, \mathrm{NO_2}, \mathrm{NH_3}$

$j =$ ads, des, fast SCR, Standard SCR, Slow SCR, NH_3 oxid., N_2O

$$\Omega_1 \dot{\theta}_1 = R_{Ads,1} - R_{Des,1} - \sum\nolimits_j N_j R_j \quad \text{Eq. (18)}$$

$$\Omega_2 \dot{\theta}_2 = R_{Ads,2} - R_{Des,2} \quad \text{Eq. (19)}$$

Equation 9 represents mass transfer from the gas stream in the channel to the surface of the catalyst. On the catalyst surface NH_3 is adsorbed onto the catalyst site in Equation 17 by Eley-Rideal mechanism from Equations 18 and 19. Equations 18 and 19 represent NH3 storage on two catalytic sites with site 1 participating in both NH_3 storage and SCR reactions and site 2 participating only in NH_3 storage.

1D DOC Model

The 1D DOC model was developed to simulate the change in NO, NO_2, hydrocarbon (HC), and carbon monoxide (CO) concentration across the DOC along with the temperature rise in the exhaust gas due to energy release by the oxidation reactions. Equations 20 and 21 represent the mass transfer from the channel gas stream to the catalyst surface and the reactions taking place on the catalytic sites.

$$\epsilon \frac{\partial c_{g,i}}{\partial t} = -\epsilon u \frac{\partial c_{g,i}}{\partial x} - \beta_i A_g \left(C_{g,i} - C_{s,i} \right) \quad \text{Eq. (20)}$$

$$\left(1 - \epsilon\right) \frac{\partial C_{s,i}}{\partial t} = -\beta_i A_g \left(C_{s,i} - C_{g,i} \right) - R_i \quad \text{Eq. (21)}$$

$i = \mathrm{CO}, \mathrm{NO}, \mathrm{NO_2}, \mathrm{C_3H_6}$

Equations 22 and 23 are used to compute the temperature change of the exhaust gas in 1D across the DOC. Equation 23 contains the energy release from the oxidation reactions. A detailed description of the model and experimental data used for calibration are given in reference [2].

$$\rho C_v \frac{\partial T_g}{\partial t} = -\rho u C_p \frac{\partial T_g}{\partial t} - h_g \frac{4}{a_w} \left(T_g - T_w \right) \quad \text{Eq. (22)}$$

$$\left(\rho_s C_{p,s}\right) \frac{\partial T_w}{\partial t} = h_g \frac{4 a_w}{a_p^2 - a_w^2} \left(T_g - T_w \right) - h_a \frac{4 a_p}{a_p^2 - a_w^2} \left(T_g - T_w \right) + \frac{A_g}{\left(1 - \epsilon\right)} \sum_{i=CO}^{HC} \frac{\Delta h_i r_i}{MW_i} \quad \text{Eq. (23)}$$

Experimental Data Overview

Experimental data from a system consisting of a Johnson Matthey SCRF® and SCR with a Cummins 2013 ISB engine was used for validating the individual models used in the proposed system. The individual SCR-F and SCR models were

TABLE 2 SCRF® + SCR system with one injector downstream of the SCRF® inlet condition.

Test point (-)	Exhaust flow rate (kg/min)	SCRF® inlet temp. (°C)	SCRF® inlet NO_2 (ppm)	SCRF® inlet NO_x (ppm)	SCRF® inlet NO_2/NO_x (-)	Inlet ANR (-)
A	5.6	267	215	590	0.44	1.10
C	6.9	339	290	689	0.44	1.02
E	7.1	342	584	1450	0.37	1.03
B	3.7	256	758	1580	0.48	1.10
D	12.5	366	161	450	0.38	1.06
1	5.2	203	182	625	0.29	1.06

calibrated as described in references [3, 5], respectively. The input data from this dataset were later used for modeling the advanced aftertreatment system consisting of SCR-F, DOC_2, and SCR with two urea injectors and decomposition tubes. The test points used for modeling each of the seven experiments from the dataset are shown in Table 2.

Table 3 shows the specifications of the aftertreatment components used for the simulations. The 1D DOC model used for the simulations was calibrated with experimental data from the 2010 ISB engine and the details of this dataset are described in reference [2].

TABLE 3 Aftertreatment component specifications.

Component	DOC and DOC_2[1]	SCR[2]	SCRF®[3]
Material	Cordierite	Cordierite	Cordierite
Catalyst	Pt	Cu-Ze	Cu-Ze
Diameter (in)	9.5	10.5	10.5
Diameter of Substrate (mm)	241.3	266.7	266.7
Length (in)	4	12	12
Length (mm)	101.6	304.8	304.8
Cell geometry	Square	Square	Square
Total volume (L)	4.65	17.04	17.04
Open volume (L)	3.5	14.04	10.2
Cell density/in^2	400	400	200
Cell width (mil)	46	46	55
Cell width (mm)	1.16	1.16	1.39
Filtration area (in^2)	N/A	N/A	11370
Open frontal area (in^2)	60	73.29	25.9
Channel wall thickness (mil)	4	4	16
Wall density (g/cm^3)	1.2	0.91	-
Porosity (%)	35	35	50
Mean pore size (µm)	N/A	N/A	16
Number of inlet cells	28353	34636	8659
Actual open surface area (m^2)	4.22	17.26	7.37
Surface area of cells (m^2)	12.08	49.33	14.74
Perimeter of cell (mm)	4.67	4.67	5.58

[1] DOC from 2010 Cummins ISB engine described in [2].

[2,3] SCR from 2013 Cummins ISB engine and SCRF® prototype from Johnson Matthey in 2014 described in [6].

Description of Aftertreatment Systems Modeled

Different combinations of the SCR-F, DOC, and SCR have been used in this research for both experimental and modeling work. Initially a DOC + SCR-F system NO_x conversion and PM oxidation characteristics were studied experimentally [6], and the 2D SCR-F model [3] was used to study the experimental data. Later a DOC + SCR-F + SCR system was modeled in reference [5]. In both these cases, a single urea injector and decomposition tube upstream of the SCR-F was used. The modeling work was then extended in this work for the two systems: 1) DOC + SCR-F + SCR system with two urea injectors and decomposition tubes and 2) DOC + SCR-F +DOC_2 + SCR system with two injectors and decomposition tubes. These two systems result in better controllability of the NO_x conversion efficiency and PM oxidation performance of the system. The details of these four aftertreatment system architectures are described in this section.

SCR-F-Only System

In a system consisting of only a SCR-F as shown in Figure 2, the SCR-F is placed downstream of a DOC and urea injector with urea mixer and decomposition tube. The urea dosed by the injector is converted to NH_3 in the decomposition tube, which then reacts with NO_x on the Cu-Ze catalyst coated inside the SCR-F substrate wall material. The SCR-F also filters the PM in the exhaust gas, which gets deposited inside the substrate wall and as a PM cake layer on top of the substrate wall. This PM undergoes oxidation by NO_2-assisted and thermal PM oxidation reactions. A competition for NO_2 between the NO_2-assisted PM oxidation reaction and the SCR reactions is observed inside the substrate wall along with forward diffusion of NO_2 from the PM cake layer to the substrate wall. The PM deposited in the wall inhibits the SCR reactions, thus reducing the effective NO_x reduction efficiency. The DOC converts NO to NO_2, which leads to a typical SCR-F

FIGURE 2 Aftertreatment system with SCR-F with one injector.

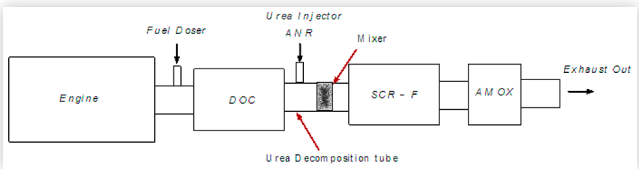

inlet NO_2/NO_x ratio of 0.35-0.4 for a range of engine operating conditions limiting the effective performance of the SCR-F in terms of NO_x reduction. These phenomena were observed experimentally and modeled using the 2D SCR-F model described in reference [3]. Based on experimental data and modeling work, an effective maximum NO_x conversion efficiency of 97.5% was observedAfor this system [3].

SCR-F + SCR with One Injector

In order to further increase the system NO_x conversion efficiency beyond the maximum value of 97.5% observed in the SCR-F-only system, an SCR was added downstream of the SCR-F with a single urea injector upstream of the SCR-F. Figure 3 shows this SCR-F + SCR system architecture. In this system an inlet ANR > 1.03 is used at the SCR-F inlet such that the NH_3 slip from the SCR-F is used as inlet NH_3 concentration for the SCR. The NO_2/NO_x ratio across the SCR-F decreases from between 0.35 and 0.4 to around 0 for all the engine operating conditions studied due to the fast SCR and NO_2-assisted PM oxidation reactions. This unfavorable SCR inlet NO_2/NO_x ratio leads to a maximum NO_x conversion efficiency of <60% for all conditions and low utilization of NH_3 leading to significant NH_3 slip [40]. The single urea injector system has limited control as compared to the two-injector system, which will be described next. This lack of control on the individual devices through urea injection is critical for cases where the SCR-F performance is significantly reduced due to ash loading and aging.

SCR-F + SCR with Two-Injector System

In order to overcome some of the limitations of a single-injection system, a system with dual injectors was modeled and evaluated. The architecture of this system is shown in Figure 4. In this system a second urea injector is added along with a decomposition tube and mixer between the SCR-F and SCR. The engine control unit (ECU) controls the signal for both the injectors, enabling greater control of the SCR-F and SCR inlet ANR value. By changing the inlet ANR values for these two injectors, the contribution of the two components in terms of NO_x conversion can be changed dynamically, based on engine operating conditions and the NOx conversion performance of the SCR-F. This setup when combined with a proper control algorithm can mitigate the reduction in SCR-F performance due to catalyst aging and ash loading by increasing the urea injection for the downstream SCR. The urea injection for the first injector will be referred to as ANR_1 and the second injector as ANR_2 for the remainder of this article.

An added benefit of this system is that the SCR-F inlet ANR can be reduced to increase the NO_2-assisted PM oxidation rate. The increase in NO_2-assisted PM oxidation in this case is due to reduced forward diffusion of NO_2 from the PM cake layer to the substrate wall, which is a function of the fast SCR reaction in the wall, and thus the SCR-F inlet ANR. The resultant reduction in NO_x conversion can be compensated by increased ANR_2 value. Up to 90%-100% increase in PM oxidation rate can be obtained with this system without significantly impacting NO_x conversion efficiency of the system. This system however is still impacted by the unfavorable NO_2/NO_x ratio at the SCR inlet (~0), limiting system maximum NO_x conversion performance.

FIGURE 3 Aftertreatment system with SCR-F + SCR with one injector.

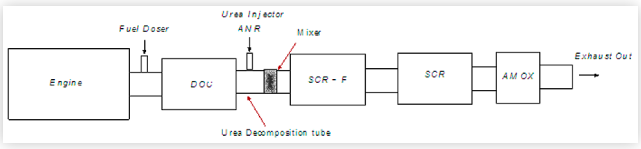

SCR-F + DOC_2 + SCR with Two Injectors

The addition of a second urea injector between the SCR-F and SCR will lead to better control of the system NO_x conversion performance by providing a way to control the conversion efficiency of the SCR-F and the SCR, and in turn the conversion efficiency of the system. However as observed in the experimental and modeling study conducted in reference [5], the consumption of NO_2 in the SCR-F by the fast SCR and NO_2-assisted PM oxidation reactions leads to a near-zero NO_2/NO_x ratio at the SCR inlet for all engine operating conditions limiting the maximum NO_x conversion efficiency of the SCR to 60%. This system limitation leads to reduced performance of both the downstream SCR even with a second urea injector. In order to overcome these limitations, new Aftertreatment system components consisting of a DOC, urea injector and decomposition tube, SCR-F, second DOC, second urea injector and decomposition tube, and downstream SCR are being proposed. In this system the second DOC, referred to as DOC_2, helps in increasing the SCR inlet NO_2/NO_x to an optimum value of 0.5 as described in reference [40]. This enables the system to reach >99.5% NO_x conversion, which will be shown in the results.

Figure 5 shows the proposed system where a second urea injector and decomposition tube was added to the system. For this system, due to the addition of a second injector, the total urea flow rate is divided into components ANR_1 and ANR_2, which represents the ANR values at the two injectors. This system increases the NO_x conversion and the PM oxidation rate over the SCR-F system alone (Figure 2). In order to achieve higher PM oxidation rate, urea injection rate in the first urea injector (based on ANR_1) is reduced for the SCR-F and to maintain the high NO_x conversion, the urea injection rate from the second injector (based on ANR_2) to the SCR is increased to maintain higher NH_3 coverage fraction (as compared to SCR-F + SCR system with one injector) in the SCR.

FIGURE 4 Aftertreatment system with SCR-F, SCR, and two urea injectors.

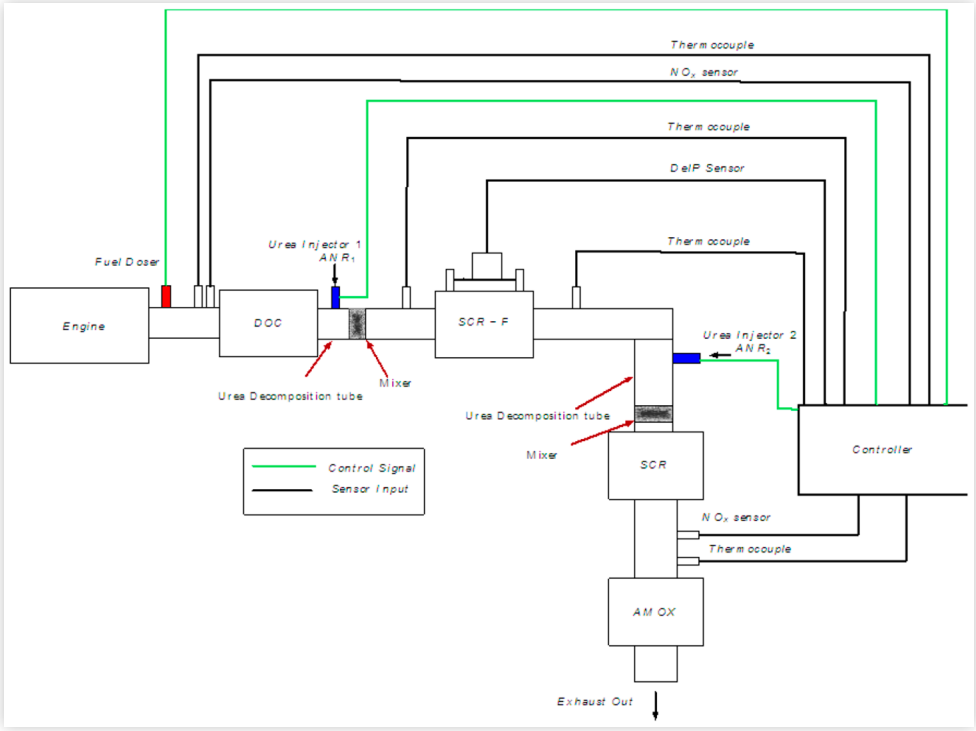

FIGURE 5 Aftertreatment system with SCR-F, a downstream DOC_2, SCR, and two urea injectors.

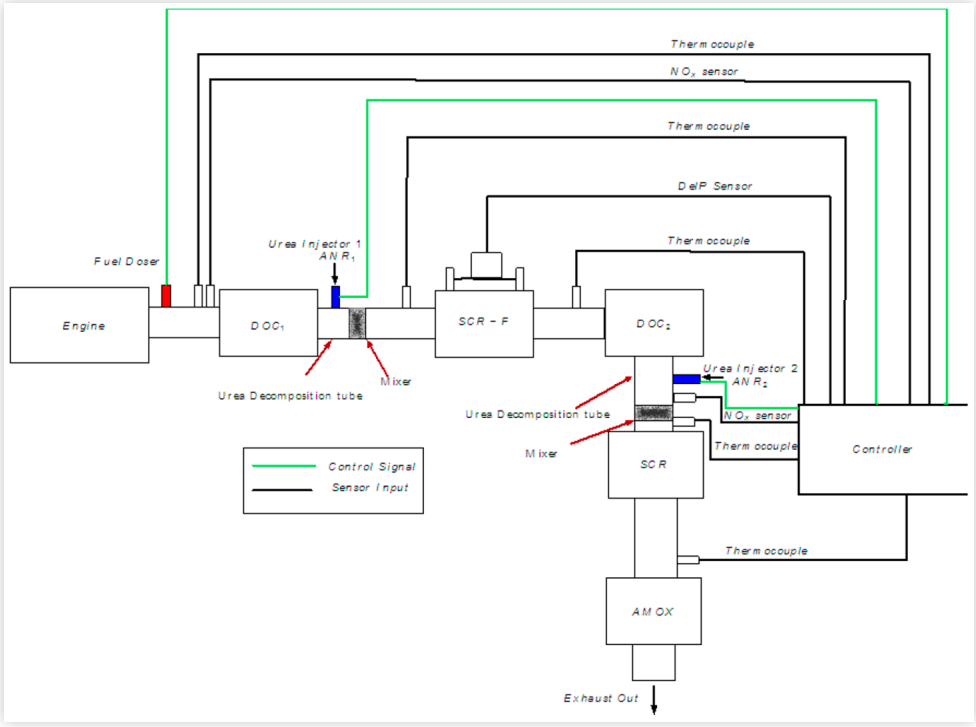

The main advantages of the proposed system are as follows:

1. Increased local NO_2/NO_x ratio to optimum values of 0.5 at downstream SCR, leading to higher fast SCR reactions and thus >99.5% system NO_x conversion.
2. Better control of inlet ANR values for both the SCR-F and the SCR, leading to accurate control of coverage fraction in both the devices.
3. Increased PM passive oxidation rate in the SCR-F using low SCR-F inlet ANR (<0.65) and up to 90% higher PM oxidation rate can be achieved, leading to a smaller number of active regeneration events which saves fuel and reduces pressure drop across the SCR-F.
4. A more robust control system results that can adapt to reduction in SCR-F NO_x conversion performance due to catalyst aging, deactivation, ash loading, and the possible issue with PGM metal transport from the DOC and deposition on the SCR-F as reported in reference [23].
5. A more robust control system results that can help in achieving better real-world emissions compliance using two injectors and a second DOC_2.

For this study only the part of the system from the SCR-F to the SCR is simulated for the hot part of the cycle.

Figure 6 shows the addition of a dCSC™ and an electric heater in place of DOC_1 shown in Figure 5. This system has the potential to meet the ultra-low NO_x standards being developed to control both the cold-start conditions and the hot part of the cycle as discussed in references [25-29]. The system consists of dCSC™ to adsorb NO_x during cold-start conditions while acting as a DOC for temperatures greater than >200°C. The dCSC™ is followed by a first urea injector and decomposition tube, and exhaust mixer. The next component in the system is the electrically heated catalyst (EHC) with control signal from the controller that can be used to heat the SCR-F for cold-start conditions to decrease the catalyst light-off time. The EHC is followed by the SCR-F, DOC_2, second urea injector, mixer and decomposition tube, and SCR.

System Model Architecture

The 2D SCR-F, 1D DOC, and 1D SCR models were used in different combinations to simulate the performance of the SCR-F, SCR-F + SCR, and SCR-F + DOC_2 + SCR systems in Figures 1, 2, 3, and 4. The system shown in Figure 5 was simulated using a combination of the 2D SCR-F, 1D DOC, and 1D SCR models. The models were run in MATLAB/Simulink in such a way that output of the first model becomes the input for the next model. The urea injection in the two injectors was controlled at a constant rate for each injector, which is given as user input for the parametric studies. In these cases, the urea is completely decomposed in the decomposition tube and the NH_3 slip from the SCR-F is assumed to be completely oxidized in the DOC_2. The engine conditions in the tests from reference [8] were used for the simulations and are shown in Table 2. The specifications of the three devices are given in Table 3, and they are described in detail in references [1, 3, 6].

FIGURE 6 Aftertreatment system with dCSC™, SCR-F, a downstream DOC_2, SCR, and two urea injectors.

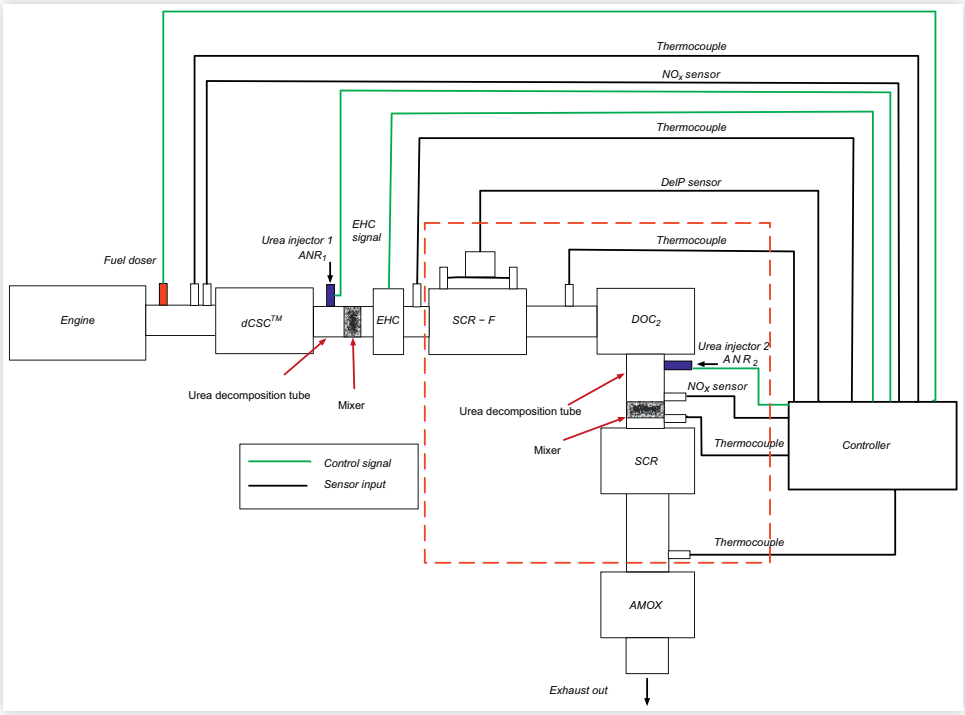

FIGURE 7 2D SCR-F + 1D DOC + 1D SCR system model.

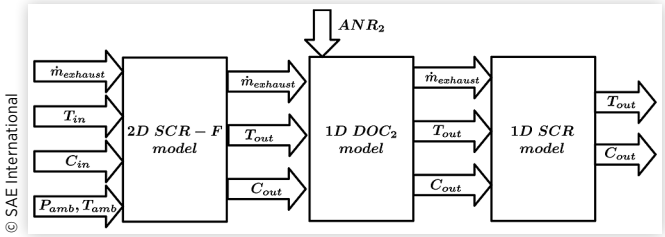

The 2D SCR-F + 1D DOC + 1D SCR system model is shown schematically in Figure 7 and was developed in MATLAB/Simulink. A variable time step solver ODE15s was used to solve for temperature, PM mass retained, and NH_3 coverage fraction states of the system components. The outlet temperature and chemical species concentrations of the SCR-F model are used as inputs for the DOC model. The NH_3 slip from SCR-F is assumed to be completely oxidized in DOC_2. The urea injector from the second injector and the DOC model outlet NO and NO_2 concentrations and the exhaust gas temperature are used as input for the 1D SCR model downstream of the DOC_2.

This system model used parameters for the models that were found using experimental data described in [2, 3, 4]. The model was able to simulate this system at a speed of 20 times the real time (1-hour data takes 180 s) on a laptop computer with 16 gb ram and quad core i7 processor. The part of the system modeled from Figure 7 is focused on modeling the physical system shown in dotted red box in Figure 6. ThisApart of the system consists of SCR-F, DOC_2, second urea injector, and SCR components. The performance of these components to only the typical steady-state engine conditions (Table 2) was simulated, and the relevant results from the simulation are presented in the results section of this article.

The system-level models described here are based on the earlier work performed on DOC + DPF and SCR-F + SCR systems that were presented in references [2, 5]. In both the cases the system models were calibrated against experimental data from 2007 ISL and 2013 ISB Cummins engines such that kinetics from earlier calibration works were able to accurately predict experimental outlet concentrations of NO_x and NH_3 to within ±20 ppm without any changes to the component model parameters. Also, for both these cases, the heat loss to ambient in the connecting pipes was neglected. The 10°-15°C temperature change leads to a ±20 ppm change in outlet NO_x concentration, which is much lower than the impact of NO_2/NO_x ratio change in the system. The results from SCR-F + SCR system study form the motivation for the work presented here. In simulations performed with heat loss in the connecting pipes, it was found that the DOC_2 has a loss of 3% for the NO oxidation rate and downstream SCR has a 0.5% drop in NOx conversion efficiency due to heat loss to the ambient due to the 6° and 10°C drop in exhaust gas temperature compared to the SCR-F inlet for these devices, respectively. Since all the simulations performed here are at steady-state engine conditions, the impact of heat loss was neglected similar to SCR-F + SCR work; however for future work involving transient data at low speeds and cold-start conditions, these heat losses needs to be taken into account. Also, further optimization of this system in terms of thermal management similar to reference [42] should further reduce the impact of heat losses in the connecting pipes.

Results

This section compares the system NO_x conversion, NH_3 slip, and urea consumed for all the four systems for one of the engine conditions (Test C in Table 2) from the data described in reference [8]. The results from Test C are described here, and the results from the remaining engine conditions are presented in Appendix A (Parametric study of engine conditions for SCR-F and SCR-F + DOC_2 + SCR systems). The models were run with different system components as shown below:

1. SCR-F (Figure 2)
2. SCR-F + SCR with one urea injector (Figure 3)
3. SCR-F + SCR with two urea injectors (Figure 4)
4. SCR-F + DOC_2 + SCR with two urea injectors (Figure 5 and part of Figure 6)

Aftertreatment system components with one urea injector represent existing prototype experimental setups that were used to collect the data for calibration of the SCR-F and SCR models. The urea injector and decomposition tube, and mixer, is present upstream of the SCR-F. The NH_3 slip from SCR-F is used as inlet concentration for the SCR-F + SCR system. These systems are constrained in terms of NO_2/NO_x ratio at the SCR-F outlet and a lack of control over the relative contribution to the NO_x system conversion by the SCR-F and SCR components.

SCR-F-Only System

In the SCR-F-only system, a SCR-F downstream of the DOC was used with a urea injector. Experimental test points with a wide range of inlet temperature (200-350°C), inlet exhaust flow rate (5-12 kg/min), and inlet NO_x (300-1600 ppm) conditions (Table 2) were used to evaluate the SCR-F performance over a wide range of ANR. The outlet DOC experimental data were used as the input data to the SCR-F. The resultant data from experimental and modeling work were analyzed and used as input for the remaining systems where the SCR-F outlet values became the inputs for the rest of the system in the simulations. The inlet urea flow rate into the SCR-F is computed using Equation 24.

$$\dot{m}_{DEF} = \frac{\dot{m}_{exh} * MW_{urea} * ANR * 1e-6 * NO_{x,in}}{0.325 * 2 * MW_{exh} * \rho_{DEF}} \quad \text{Eq. (24)}$$

$$MW_{exh} = \sum_{i=1}^{4} Y_i * MW_i \quad \text{Eq. (25)}$$

The change in the SCR-F outlet NO, NO_2, and NH_3 concentrations as a function of SCR-F inlet ANR is shown in Figure 8. Test C was used for this figure with SCR-F inlet ANR on the x axis with a range of 0 to 1.2. The experimental data for this test is shown in circles. The left-hand y axis shows the outlet concentration while the right-hand side y axis shows the SCR-F outlet NO_2/NO_x ratio. With an increase in the inlet ANR value, the NO and NO_2 decrease for the entire ANR range. The outlet NO_2 reaches zero concentration for ANR > 0.8 and the NO reaches a value of 30 ppm at ANR = 1.2. The outlet NH_3 concentration is near zero for ANR < 0.8, and beyond this ANR, a significant rise in NH_3 slip is observed. The SCR-F outlet NO_2/NO_x reaches a value of zero for inlet ANR > 0.8 due to the consumption of NO_2 by both fast and slow SCR reactions.

The near-zero SCR-F outlet NO_2/NO_x concentration for ANR > 0.8 represents a typical operating condition of the DOC + SCR-F system. This low value constraints the maximum performance of the downstream SCR in a SCR-F + SCR system, limiting it to a maximum conversion efficiency of 98.5% as described in reference [5].

In Figure 9 the NO_x conversion increases with an increase in the inlet ANR value, reaching a maximum value of 98.6% at ANR 1.2. The SCR-F maximum NO_x conversion efficiency is limited by the exhaust flow rate, temperature, and inlet NO_2/NO_x ratio conditions from Figure 8 for the given engine condition. The impact of the PM cake on the local NO_2/NO_x ratio in the substrate wall and inhibition of the SCR reactions due to the wall PM [3] have also been taken into account for these data. The urea flow rate has a linear relationship with the inlet ANR increasing from inlet ANR = 0-1.2. The PM oxidation rate decreases with an increase in the inlet ANR due to an increase in the forward diffusion rate of the NO_2 from the PM cake to the substrate wall.

The SCR-F and SCR models were calibrated against a range of ANR values (0.8 to 1.2) and in a temperature range

FIGURE 8 Outlet concentrations and SCR-F outlet NO_2/NO_x ratio vs. inlet ANR values at engine condition C (SCR-F with one Urea injector).

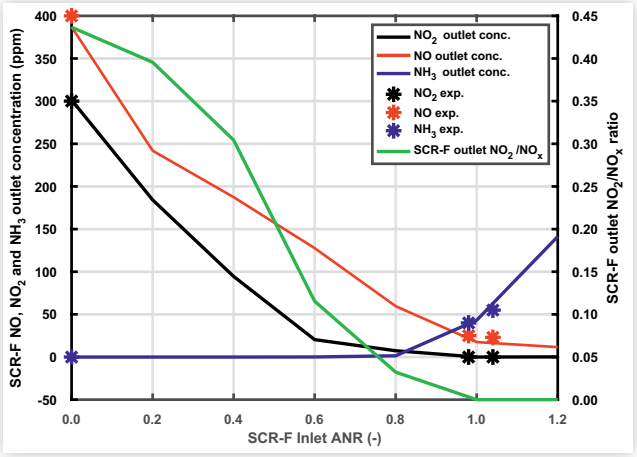

FIGURE 9 NO_x conversion efficiency, urea flow rate, and PM oxidation rate vs. SCR-F inlet ANR at engine condition C (SCR-F with one Urea injector).

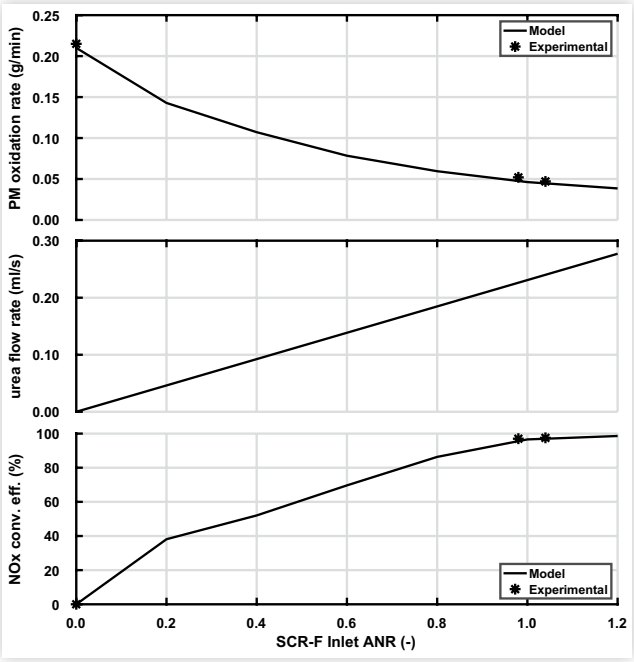

of 200-450°C. These results were presented in references [3, 6]. Further work on SCR-F + SCR system was performed in reference [5], where the kinetics from the earlier work was used to simulate the outlet NO_x and NH_3 concentrations. These experiments were conducted at ANR of 1 and 1.1, which have been presented in Figures 8 and 9. The calibrated SCR-F and SCR models were able to simulate outlet NO_x and NH_3 concentrations to within ±20 ppm in ANR range of 0.8 to 1.2, temperature range of 200-450°C, and at 0, 2, and 4 g/l PM loading for the SCR-F. The SCR-F model was able to accurately simulate the experimental PM oxidation rate and NO_x conversion efficiency at ANR = 0 from reference [7]. The ANR = 0 comparison is shown in Figure 9, further validating the kinetics of the model for the ANR = 0. Due to this, the authors believe that the models have the fidelity to accurately simulate the PM oxidation rate and SCR reactions for the ANR range of 0 to 1.2, which forms the basis for the results presented.

SCR-F + SCR with One Urea Injector

The SCR-F + SCR system components (Figure 3) with one urea injector were modeled with an inlet ANR value of 1 to 1.12 at the inlet of the SCR-F (Figure 8), with the SCR-F NH_3 outlet concentration being used as the inlet NH_3 for the SCR. Figure 10 shows the results from these simulations. The steep slope of the NH_3 outlet concentrations for ANR > 1.0 from Figure 8 shows that the control system must be precise in

FIGURE 10 NO_x conversion efficiency, urea flow rate, and outlet concentrations vs. SCR-F inlet ANR at engine condition C (SCR-F + SCR with one urea injector).

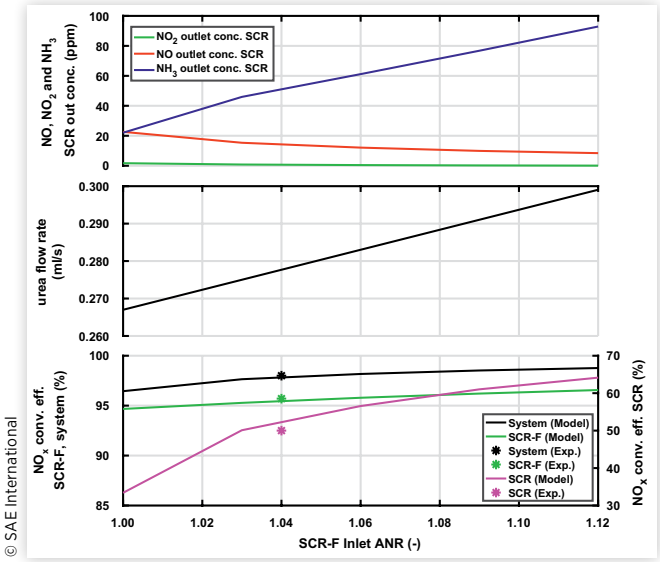

setting the SCR-F inlet ANR so as to not have excess slip or lower NO_x conversion efficiency.

The NO_x conversion of the SCR-F + SCR system components increases with an increase in the SCR-F inlet ANR reaching a maximum value of 99% at ANR = 1.12. The addition of the SCR leads to the 0.4% increase in the system NO_x conversion efficiency compared to the SCR-F-only system. The SCR efficiency is limited by the NO_2/NO_x ratio from Figure 8 at the inlet of the SCR due to the SCR-F near-zero NO_2 outlet concentration, leading to a lower SCR NOx conversion efficiency due to only the standard SCR reaction. Since the SCR inlet NH_3 is a function of the SCR-F NH_3 outlet concentration, the efficiency of the SCR is less than 50% for values of ANR < 1.03 due to the low SCR-F NH_3 outlet concentration. When the NH_3 concentration increases, the SCR and system NO_x conversion efficiencies increase resulting in the slope change observed in the NO_x conversion efficiency plots at ANR = 1.03. The urea flow rate increases linearly with an increase in the inlet SCR ANR value, which reaches a maximum urea flow rate of 0.297 ml/s at ANR = 1.12

The SCR outlet NO_2 is near zero for all values of ANR as the SCR-F outlet NO_2 is zero. The SCR NO outlet concentration decreases to less than 10 ppm at ANRs greater than 1.09 as a result of the standard SCR reaction. The standard reaction starts reducing NO at ANR = 1.03 where the SCR-F NH_3 outlet concentration (Figure 8) is over 70 ppm. The outlet NH_3 concentration of the system increases with ANR value to a maximum value of 92 ppm at ANR = 1.12 (Figure 10). The high NH_3 slip is due to the mass transfer limitations, and 65% maximum efficiency of the SCR is a result of the unfavorable SCR inlet NO_2/NO_x ratio (Figure 8).

The addition of the second injector enables better control on the individual performance of the SCR-F and SCR. A second advantage with this system is significant increase in SCR-F PM oxidation rate by reducing the urea injection at the SCR-F inlet.

The systems with two injectors (ANR_1 and ANR_2) lead to a concept of system ANR which represents the ratio of the total NH_3 produced from the urea flow rate at the two injectors divided by the NO_x concentration at the inlet of the SCR-F. The system ANR is defined by Equation 26.

$$ANR_{system} = \frac{\left(ANR_1\ NO_{x,in,SCR-F} + ANR_2\ NO_{x,in,SCR}\right)}{NO_{x,in,SCR-F}} \quad \text{Eq. (26)}$$

where ANR_1 is the ANR at urea injector 1 and $NO_{x,in,SCR-F}$ is NO_x SCR-F inlet concentration. ANR_2 is the ANR at urea injector 2 and $NO_{x,in,SCR}$ is NO_x SCR inlet concentration.

SCR-F + SCR with Two Urea Injectors

The SCR-F + SCR with two-injector system was run with the second urea injector at the inlet of the SCR with ANR_2 in a range of 1-1.12 to evaluate the system performance. The NH_3 outlet concentration from the SCR-F and the NH_3 decomposed from the urea injected from the second urea injector were used as the inlet NH_3 for the SCR. Figure 11 shows the results from the system simulation.

The NO_x conversion efficiency is comparable to the SCR-F + SCR system with one Urea injector with an efficiency of

FIGURE 11 NO_x conversion efficiency, urea flow rate and outlet concentrations vs. SCR-F inlet ANR_2 at engine condition C and for ANR_1 0.6 and 0.7 (SCR-F + SCR with two urea injectors).

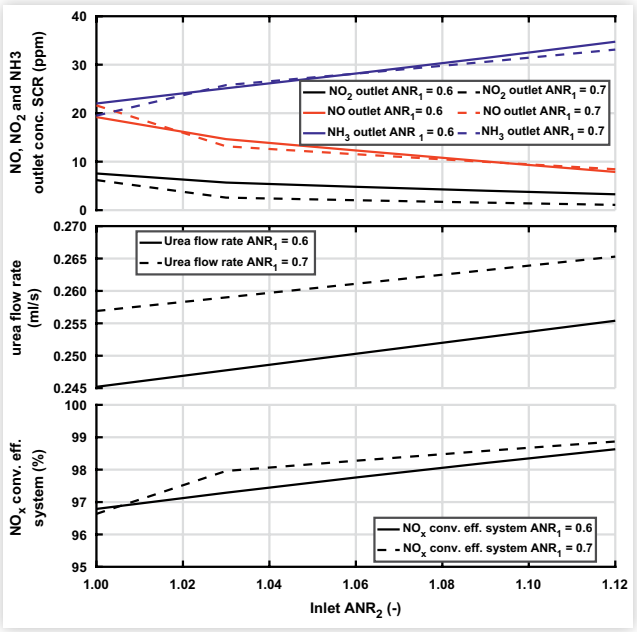

99.0% at ANR_1 = 0.7 and ANR_2 = 1.12. The SCR conversion efficiency is limited by the low NO_2 concentration at the inlet of the SCR leading to a SCR NO_x conversion efficiency of 85% at ANR_2 = 1.12. The urea flow rate at ANR_2 =1.12 for the ANR_1 = 0.7 case is 0.284 ml/s. The addition of a second injector enables the operation of the SCR-F at ANR_1 = 0.7, which gives better control of the NH_3 coverage fraction in both the SCR-F and SCR.

SCR-F + DOC_2 + SCR with Two Urea Injectors

For the two systems, the SCR-F + SCR (Figure 4) and SCR-F + DOC_2 + SCR (Figure 5 and Figure 6 - red line) systems, a second Urea injector was added to enable better control of the NH_3 coverage fraction in both the SCR-F and SCR. In order to control these systems, the ANR values for urea injection at the two injectors (ANR_1 and ANR_2) are determined from the control algorithm based on exhaust NO_x concentration, temperature, and exhaust flow rate from the sensors and PM retained in the SCR-F estimator.

The SCR-F + DOC_2 + SCR system was run with ANR_1 in the range of 0-1.0 in Figure 12, in order to determine a good operating range of ANR_1. ANR_2 was determined in such a way that total urea flow rate is constant (0.258 ml/s) for all values of ANR_1 and ANR_1 = 0.65 and ANR_2 = 1.07 for this flow rate. The ANR_2 values shown in this figure were calculated based on maximizing the NO_x conversion efficiency while keeping the total urea flow rate constant for the given ANR_1 value. Figure 12 shows the change in the system NO_x conversion efficiency, ANR_2, PM oxidation rate, SCR-F outlet NO_2, and SCR outlet NH_3 concentrations as a function of ANR_1.

The system NO_x conversion efficiency increases from ANR_1 = 0.0-0.65 reaching a maximum value of 99.9%. The ANR_2 also decreases with increase in ANR_1, reaching a minimum value of 1.03. The PM oxidation rate decreases with an increase in ANR_1 due to the forward diffusion of the NO_2 from the PM cake to the substrate wall in the SCR-F with an increase in ANR_1 value.

The outlet SCR-F NO_2 concentration decreases with an increase in ANR_1 and the values beyond ANR_1 = 0.65 being less than 15 ppm. The SCR NH_3 outlet concentration follows the trend of the system NO_x conversion efficiency with a minimum NH_3 outlet concentration at ANR_1 = 0.65 where highest NO_x conversion was observed. Based on the trends in Figure 8, the PM oxidation rate can be increased further by using ANR_1 values less than 0.6 if a lower NO_x conversion efficiency is acceptable for a given engine load and speed condition. At ANR_1 = 0.0 the NO_x conversion efficiency of the system decreases to 94%. The region of ANR_1 greater than 0.7 is undesirable for operation for this engine condition since it offers neither an increase in PM oxidation rate nor improved NO_x conversion efficiency.

In order to determine the reason behind the trend in NO_x conversion efficiency in Figure 12, the NO_2/NO_x ratio at the outlet of the SCR-F and the DOC_2 were plotted against ANR_1 as shown Figure 13.

As can be observed in Figure 13, the addition of DOC_2 leads to the NO_2/NO_x ratio increase compared to the SCR-F outlet value. This increased NO_2/NO_x ratio is the inlet NO_2/NO_x ratio for the SCR. The DOC_2 outlet NO_2/NO_x ratio starts at 0.69 and decreases to 0.5 for an ANR_1 of 0.6. There is a further decrease in DOC_2 outlet NO_2/NO_x ratio with an increase in ANR_1 value following the trend of the SCR-F outlet

FIGURE 12 NO_x conversion efficiency, ANR_2, PM oxidation rate, SCR-F outlet NO_2, and SCR outlet NH_3 concentration vs. ANR_1 at engine condition C (SCR-F + DOC_2 + SCR with two urea injectors).

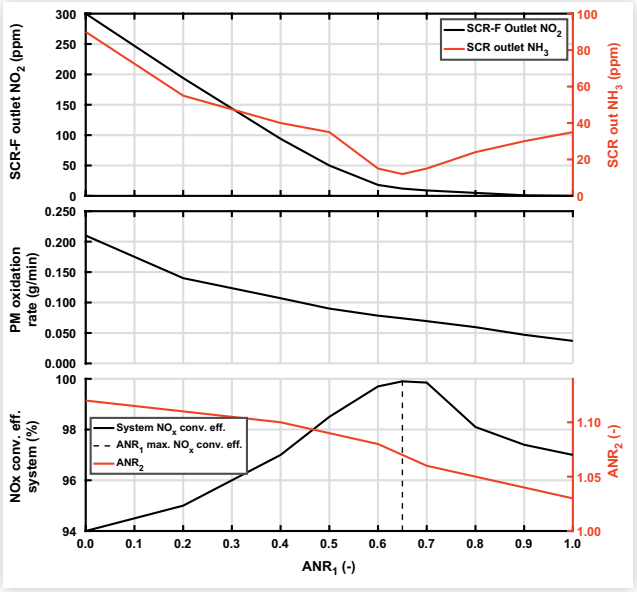

FIGURE 13 NO_2/NO_x ratio vs. ANR_1 at engine condition C (SCR-F + DOC_2 + SCR with two urea injectors).

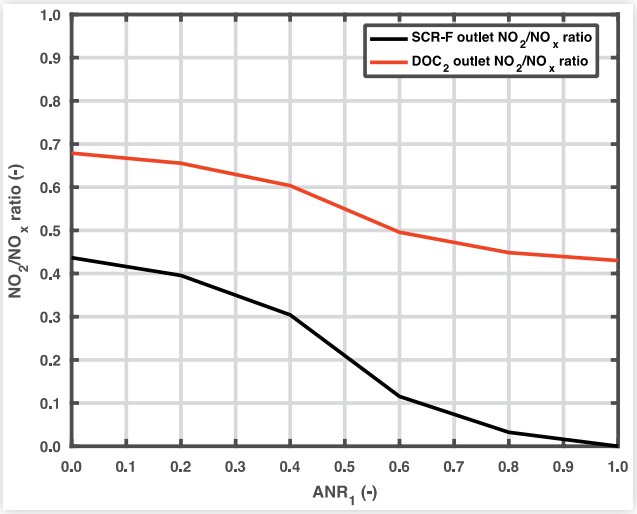

NO_2/NO_x ratio, but this is in the ANR_1 region where operation is not desirable.

For ANR_1 = 0.65, the SCR efficiency increases to 97% from the 71% in the system without DOC_2 (Figure 10, ANR = 1.12) due to the favorable NO_2/NO_x ratio of 0.5 [4]. This leads to a system NO_x conversion efficiency of 99.9% for ANR_1 = 0.65 and ANR_2 = 1.06.

Based on Figures 10 and 11, an ANR_1 of 0.6 and 0.7 with ANR_2 from 1 to 1.12 were chosen for simulating the SCR-F + SCR (with two Urea injectors) and the SCR-F + DOC_2 + SCR (with two Urea injectors) systems, as it represented ANR_1 values which provided the highest system NO_x conversion efficiency.

The SCR-F + DOC_2 + SCR (Figure 5) system components consist of two urea injectors similar to the SCR-F + SCR (Figure 4) system with two Urea injectors; however in this system a DOC_2 is added between the SCR-F and the SCR, as shown in Figure 5, to oxidize NO to NO_2 enabling favorable NO_2/NO_x ratios (0.5-0.6) at the inlet of the SCR. The DOC_2 also oxidizes the outlet NH_3 concentrations from the SCR-F, and NH_3 from the SCR-F is negligible for ANR_1 values below 0.7, as seen in Figure 9. These simulations were run with ANR_1 of 0.6 and 0.7 and ANR_2 of 1 to 1.12 similar to the SCR-F + SCR system. Results from these simulations are shown in Figure 14.

The NO_x conversion efficiency is comparable to the SCR-F + SCR system with one Urea injector with an efficiency of 99.0% at ANR_1 = 0.7 and ANR_2 = 1.12. The SCR conversion efficiency is limited by the low NO_2 concentration at the inlet of the SCR (Figure 11), leading to a SCR NO_x conversion efficiency of 85% at ANR_2 = 1.12. The urea flow rate at ANR_2 =1.12 for the ANR_1 = 0.7 case is 0.284 ml/s. The addition of a second injector enables the operation of the SCR-F at ANR_1 at 0.7 which gives better control of the NH_3 coverage fraction in both the SCR-F and SCR. This leads to a higher PM oxidation rate in the SCR-F in this system as compared to the system with one Urea injector.

The NO_x conversion efficiency is higher for this system with a maximum efficiency of 99.9% for ANR_1 = 0.7 at ANR_2 = 1.12. This system is not limited by the low NO_2 concentration from the SCR-F outlet since the DOC_2 for this engine condition converts 60% of the SCR-F outlet NO to NO_2. The near 100% efficiency for ANR_1 = 0.7 is due to the favorable NO_2/NO_x ratio into the SCR. The outlet SCR NO_2 concentration for at ANR_1 = 0.7 is near zero with NO concentrations being less than 6 ppm. The NH_3 slip was also observed to be lower than the SCR-F + SCR system with two Urea injectors due to the higher utilization of the NH_3 for NO_x reduction with a maximum NH_3 slip of 20 ppm. The urea flow rate for this system ANR_1 = 0.7 and ANR_2 = 1.12 is 0.172 and 0.085 ml/sec for injections 1 and 2, respectively, with total flow rate = 0.284 ml/s.

Comparison of the Four Systems

The four systems were run with system ANR of 1.007-1.037. For systems with one injector, ANR_2 = 0 and ANR_{system} = ANR_1. The PM oxidation rate, urea flow rate, and NO_x conversion efficiency have been compared for these four systems in Figure 15.

As observed from Figure 15, the NO_x conversion efficiency of the SCR-F-only system was observed to be 97.5% at

FIGURE 14 NO_x conversion efficiency, urea flow rate, and outlet concentration vs. SCR-F inlet ANR at engine condition C (SCR-F + DOC_2 + SCR with two urea injectors).

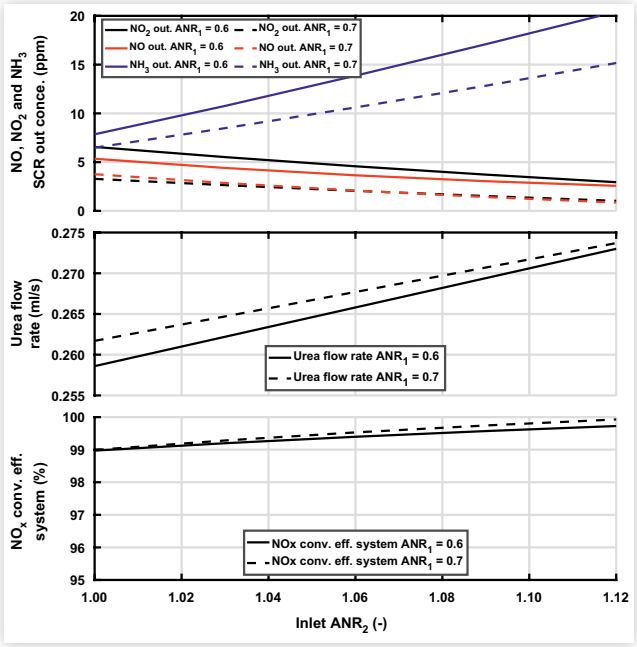

FIGURE 15 NO_x conversion efficiency, urea flow rate, and PM oxidation rate vs. system inlet ANR at engine condition C.

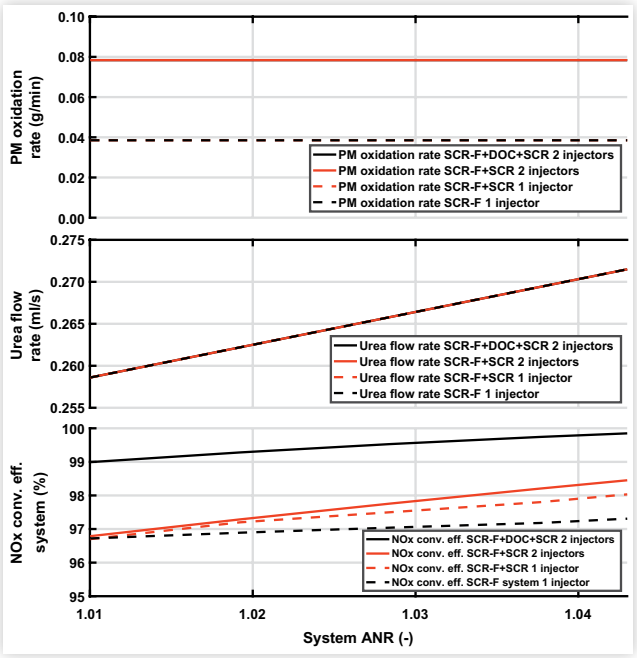

system ANR of 1.027, the SCR-F + SCR with one injector has an efficiency of 97.5%, and followed by SCR-F + SCR system with two injectors with 97.8%. The SCR-F + DOC_2 + SCR system had the higher NO_x conversion efficiency of 99.5%. The SCR-F + DOC_2 + SCR system due to the favorable NO_2/NO_x ratio in the SCR consistently leads to a further improvement from 97% to 99% as was observed compared to SCR-F-only system, which is 67% of the remaining 3% NO_x. The urea flow rate is the same for all the cases and is linearly proportional to the system ANR. For a given amount of urea flow rate, the SCR-F + DOC_2 + SCR system has higher NO_x conversion efficiency (99.9% efficiency at $ANR_1 = 0.65$ and $ANR_2 = 1.06$) than the remaining systems, which can be used to reduce the urea consumption if a lower NO_x conversion efficiency is acceptable for a given engine condition, and it is desirable to increase the PM oxidation rate.

The PM oxidation rate in Figure 15 shows a trend where the systems with two urea injectors at $ANR_1 = 0.7$ have oxidation rates of 0.079 g/min compared to 0.039 g/min for systems with one urea injector. The reduction in urea injection for the SCR-F in a dual-injector system leads to a higher PM oxidation rate in the SCR-F as compared to the system with one Urea injector. This 100% improvement in the PM oxidation rate is due to the lower forward diffusion rate at lower ANR_1 values leading to higher available NO_2 in the PM cake and higher PM oxidation rate. This trend is consistent with the PM oxidation rate vs. inlet ANR of the SCR-F-only system from Figure 9.

Analysis of Results

Table 4 compares the performance of the four systems for a system of ANR = 1.04, $ANR_1 = 0.65$, and $ANR_2 = 1.06$ for the systems with two Urea injectors at engine condition C. The values of ANR_1 and ANR_2 for the dual-injector systems were chosen based on the trends from Figure 11. As shown in Table 4, there is 2.1% increase in the NO_x conversion efficiency for the system with DOC_2 compared to SCR-F-only system. The systems with two injectors have 80% higher PM oxidation rate. The NH_3 slip value for the system with a DOC_2 is 14 ppm compared to 75 ppm for the SCR-F-only system due to better utilization of NH_3 in the SCR. The urea flow rate is 1.4% lower in the case of the system with the DOC_2 (0.275 vs. 0.276 ml/s) due to lower NH_3 slip and better NH_3 utilization.

TABLE 4 Performance of the four systems at system ANR = 1.04.

Units	NO_x conv. efficiency %	PM oxid. rate g/min	NH_3 slip ppm	Urea flow rate ml/s
SCR-F-only 1 injector (ANR1 = 1.04, ANR2 = 0)	97.8	0.039	75	0.276
SCR-F + SCR 1 injector ($ANR_1 = 1.04$, $ANR_2 = 0$)	98	0.039	50	0.276
SCR-F + SCR 2 injectors ($ANR_1 = 0.65$, $ANR_2 = 1.06$)	98.5	0.07	22	0.275
SCR-F + DOC_2 + SCR 2 injectors ($ANR_1 = 0.65$, $ANR_2 = 1.06$)	99.9	0.07	14	0.274

TABLE 5 SCR-F + DOC_2 + SCR system performance for maximum NO_x conversion efficiency.

Maximum NO_x conversion efficiency						
Engine condition	(-)	1	A	C	D	E
ANR_1	(-)	0.72	0.8	0.65	0.8	0.8
ANR_2	(-)	1.04	1.03	1.06	1.04	1.03
Urea flow rate in injector 1	(ml/s)	0.109	0.391	0.172	0.209	0.408
Urea flow rate in injector 2	(ml/s)	0.047	0.102	0.085	0.058	0.106
Total urea flow rate	(ml/s)	0.156	0.493	0.258	0.268	0.513
System NO_x conversion efficiency	(%)	99.3	99.8	99.9	99.2	99.8
SCR-F PM oxidation rate	(g/min)	0.01	0.013	0.07	0.036	0.04
SCR NH_3 slip	(ppm)	39	24	14	28	19

Tables 5 and 6 show the system performance at the engine conditions as given in Table 2 and based on the figures in the Appendix A for the maximum NO_x conversion and the maximum PM oxidation, respectively, for engine conditions 1, A, C, D, and E.

As can be observed from Table 5, the NO_x conversion efficiency of the SCR-F + DOC_2 + SCR system is over 99.2% for all the engine conditions. The value of ANR_1 is in the range of 0.65 to 0.8 (0.72±0.08) depending on PM oxidation rate in the SCR-F, exhaust temperature, NO and NO_2 concentrations at the SCR-F inlet, and exhaust flow rate conditions. The ANR_2 has a much narrower range of 1.03 to 1.07 (1.04±0.02), and the system is less sensitive to a change in the ANR_2 value compared to ANR_1. The NH_3 slip values observed in Table 5 will be reduced to meet EPA standards by the AMOX placed

TABLE 6 SCR-F + DOC_2 + SCR system performance for maximum PM oxidation rate at $ANR_1 = 0$.

Maximum PM oxidation rate with PM loading 2 g/l						
Engine condition	[-]	1	A	C	D	E
ANR_2	[-]	1.12	1.12	1.12	1.12	1.12
Urea flow rate in injector 2	[ml/s]	0.169	0.548	0.297	0.293	0.571
System NO_x conversion efficiency	[%]	93.5	91.5	94	91	94.9
SCR-F PM oxidation rate	[g/min]	0.041	0.057	0.21	0.13	0.5
SCR NH_3 slip	[ppm]	80	70	83	60	90

downstream of the SCR in the system which hasn't been modeled in this work.

In Table 6, the ANR_2 value for all cases is 1.12 in order to maximize the NO_x conversion efficiency, while the PM oxidation rate in the SCR-F is the maximum possible value for the given engine condition. A higher NH_3 slip is also observed compared to the Table 4 data at the same engine condition. The PM oxidation rates are three to four times higher than the values from Table 4, so these $ANR_1 = 0$ conditions can be used where a higher PM oxidation rate is desired while having a reduced NO_x reduction performance. The only way the SCR-F-only system can increase the PM oxidation rate is to reduce the ANR through the SCR-F with a significant loss of NO_x conversion efficiency (40% at ANR = 0.2 vs. 85% at ANR = 0.8 in Figure 9).

Table 7 compares the performance of the SCR-F-only system with the SCR-F + DOC_2 + SCR system for maximum NO_x conversion efficiency. As observed in Table 7, the SCR-F + DOC_2 + SCR system has 1.8%-8.3% higher NO_x conversion efficiency compared to the SCR-F-only system. The NH_3 slip was observed to be 20-174 ppm in SCR-F-only system compared to 17-39 ppm in SCR-F + DOC_2 + SCR system due to better utilization of the NH_3. The total urea flow rate was also observed to be 1%-3% higher in the SCR-F system while the PM oxidation rate is 140%-300% higher in the SCR-F + DOC_2 + SCR system compared to the SCR-F only.

The conclusions from the results with engine condition C are

1. SCR-F + SCR (one Urea injector) system components, as compared to the SCR-F-only system, result in slightly improved NOx conversion efficiency and lower NH_3 slip without an improvement in the PM oxidation rate for engine condition C (Table 4).
2. The SCR-F + SCR (two Urea injectors) system components as compared to the SCR-F + SCR (one Urea injector) system result in a slightly improved NO_x conversion efficiency and lower NH_3 slip with a 80% improvement in the PM oxidation rate for engine condition C (Table 4), because it is possible to operate at $ANR_1 = 0.65$ with this dual-injector system.
3. The SCR-F + DOC_2 + SCR system (two Urea injectors) components as compared to the SCR-F + SCR (two Urea injectors) system result in a 1.4% improvement in the NO_x conversion efficiency and lower NH_3 slip and the same PM oxidation rate for engine condition C (Table 4), because the DOC_2 improves the NO_2/NO_x ratio in the 0.5-0.6 range for optimum NO_x reduction.
4. For both of the dual-injector systems components (SCR-F + DOC_2 + SCR and SCR-F + SCR), the PM oxidation rate is 80% higher at $ANR_1 = 0.65$ while achieving 99.9% NO_x conversion for the SCR-F + DOC_2 + SCR system compared to the SCR-F-only system for engine condition C (Table 4). A further gain in PM oxidation rate can be obtained by decreasing the ANR_1 between 0.65 and 0, if an increased PM oxidation rate and decreased NO_x conversion rate is desired. Neither of the single injector systems (SCR-F, SCR-F + SCR) can achieve this level of PM oxidation rate with over 90% NO_x conversion efficiency.

TABLE 7 SCR-F vs. SCR-F + DOC_2 + SCR systems performance for maximum NO_x conversion efficiency.

Engine condition	-	1	A	C	D	E
ANR	-	1.06	1.05	1.07	1.06	1.08
Total urea flow rate	ml/s	0.16	0.514	0.284	0.277	0.55
System NO_x conv. effi.	%	91	97.6	97.4	95	98
SCR-F PM oxid. rate	g/min	0.001	0.005	0.04	0.012	0.028
System NH_3 slip	ppm	41	25	80	97	174
ANR_1/ANR_2	-	0.72/1.04	0.80/1.03	0.65/1.07	0.80/1.04	0.80/1.03
Total urea flow rate	ml/s	0.156	0.493	0.258	0.268	0.513
System NO_x conv. effi.	%	99.3	99.8	99.9	99.2	99.8
SCR-F PM oxid. rate	g/min	0.01	0.013	0.07	0.036	0.04
System NH_3 slip	ppm	39	24	17	28	19

The conclusions from results for all engine conditions are

1. For all engine conditions ANR_1 was found to be 0.72±0.08 and ANR_2 was 1.04±0.02 for maximum NO_x conversion efficiency for the SCR-F + DOC_2 + SCR system components (Table 5). It appears that the ECU controller should be able to easily control these two urea flow rates that are mainly a function of the NO_x concentrations and exhaust flow rates from the sensors (Figure 5 and Figure 6).
2. Table 6 shows the maximum PM oxidation rate that can be achieved by the SCR-F + DOC_2 + SCR system components using $ANR_1 = 0$ for all engine conditions. The PM oxidation rate is three to four times higher than the oxidation rate for the SCR-F system at the same engine conditions. This change in ANR_1 can be used for engine and PM loading conditions where high PM oxidation rate and a NO_x conversion efficiency greater than 91% are desirable.
3. The SCR-F + DOC_2 + SCR system components has 1.8%-8.3% higher NO_x conversion efficiency and 140%-300% higher PM oxidation rate with 1%-3% lower urea flow rate and 2-150 ppm lower NH_3 slip for all engine conditions at maximum NO_x conversion efficiency compared to the SCR-F system (Table 7).

SCR-F + DOC_2 + SCR Control System

The SCR-F + DOC_2 + SCR system components described in Figure 5 and Figure 6 require a control system that will

be implemented in the ECU (controller) to determine the amount of urea to be injected in both the urea injectors based on the given exhaust flow rate, exhaust gas temperature, engine-out NO and NO_2 concentration, and SCR-F PM loading.

The control system consists of DOC, SCR-F, DOC_2, and SCR state estimators that are coupled to estimate the states of PM mass retained, NH_3 coverage fraction, and exhaust inlet temperatures. The exhaust gas chemical species concentrations change as the exhaust flows through each of the devices. This variation in chemical species concentration of NO, NO_2, and NH_3 is also computed and tracked by the four estimators. These data are then used by the control algorithm to control the PM oxidation rate in the SCR-F and the system, and the SCR-F and the SCR NO_x conversion efficiencies. A detailed description of the DOC and SCR estimators are given in reference [2] with SCR-F estimator in reference [41]. It should be noted that alternative state estimators could be used such as neural networks or other machine learning techniques. Figure 16 describes the flowchart for the complete system that can be used to determine the desired urea flow rate for the two urea injectors based on the control algorithm.

The control algorithm determines the ANR_1 and ANR_2 values based on the engine map to determine the PM oxidation rate in the SCR-F and the system, and the SCR-F and the SCR NO_x conversion efficiencies based on the desired reaction rates with respect to engine-out temperature; NO, NO_2, and PM concentrations; and PM mass retained in the SCR-F. This control algorithm can be configured to either maximize NO_x conversion efficiency, minimize urea consumption, maximize the PM oxidation rate in the SCR-F, or any combination of these objectives based on engine-out exhaust temperature and flow rate, pressure drop in the SCR-F, PM loading, NO_x concentration for a given engine speed, and load condition.

The control system described here is based on state estimators developed in references [2, 41]. Its aim is to maximize the performance of the proposed system for a given set of requirements and engine conditions. The scope of this work only provides a brief description of a potential control system. Future work on this system would provide a detailed quantitative and qualitative analysis of this control system. This article focuses on simulating steady-state engine conditions, and there was to not to model the control system.

FIGURE 16 DOC + SCR-F + DOC_2 + SCR control system flowchart.

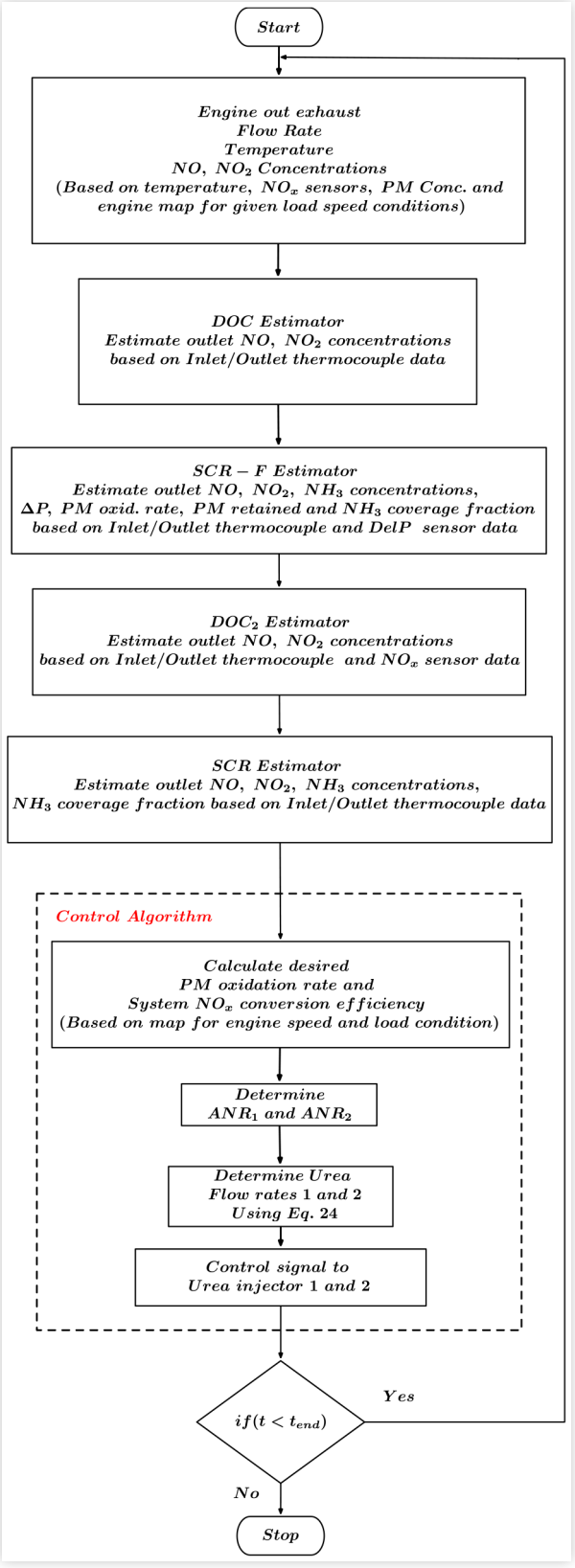

Summary/Conclusions

The advantages of the SCR-F + DOC_2 + SCR system components (two Urea injectors) as compared to the SCR-F system are

1. The system has a 99.2% to 99.9% NO_x conversion efficiency as compared to 91.0%-98.0% for the SCR-F only for all the engine conditions (Table 7).
2. The system has a 0.013-0.070 g/min PM oxidation rate as compared to 0.005-0.040 g/min for the SCR-F only for all the engine conditions (Table 7).

3. The system has a 17-39 ppm NH_3 slip as compared to 20-174 ppm for the SCR-F only for all the engine conditions (Table 6).
4. The SCR-F + DOC_2 + SCR system components enable three to four times higher PM oxidation rate as compared to the SCR-F system (Tables 5 and 6) when $ANR_1 = 0$, which is used in engine conditions where a higher PM oxidation rate and 91%-95% NOx conversion efficiency are desirable (Table 5). The only way the SCR-F-only system can increase the PM oxidation rate is to reduce the ANR to the SCR-F with a significant loss of NO_x conversion efficiency (40% at ANR = 0.2 vs. 85% at ANR = 0.8 in Figure 9).
5. The trade-off between PM oxidation rate and NO_x conversion efficiency can be determined by the control algorithm in the SCR-F + DOC_2 + SCR system based on the engine map for a given engine speed and load condition. The control system can also operate over a limited range of ANR_1 (0.72±0.08) and ANR_2 (1.04±0.02) conditions for the engine conditions stated without a loss in NO_x conversion efficiency and PM oxidation rate, enabling a more robust control system. This control cannot be achieved in the SCR-F-only system.

The systems described in Figures 3 and 4 and the performance of these systems is based on existing DOC, SCR-F, and SCR components described in Table 3. The catalyst loading of each device can also be modified along with sizing of the components to better optimize for various engine applications and to improve the PM oxidation rate, NH_3 slip, and the NO_x conversion efficiency including the volume and cost of the individual components and the system. The estimator models used for the control system design and sensor layout can also be modified to make the system more suitable for a given application.

The DOC and DOC_2 are flow-through devices that can be designed to consist of different types of catalysts such as platinum, palladium, rhodium, barium, which can be used to absorb, adsorb, and oxidize HCs, CO, and NO present in the exhaust gas. The oxidation of NO to NO_2 is one of the main reactions that will be used in the DOC and DOC_2 in the proposed system to improve the system NO_x conversion efficiency.

The SCR-F is a wall flow-type device which can contain different types of catalysts such as vanadium, Cu-Ze, iron zeolite and different physical structures and cell designs consisting of porous materials. The catalyst is responsible for adsorption of reductants such as NH_3 and reduction of NO_x to nitrogen and water vapor using the SCR reactions. The physical structure of the SCR-F can also be comprised of different materials such as silicon carbide, other ceramics, metallic meshes, or any form of porous material. The SCR uses similar catalysts as the SCR-F in a flow-through setup to reduce NO_x emissions in the exhaust gas into nitrogen and water vapor by SCR reactions. The AMOX downstream of the SCR is responsible for oxidation of outlet NH_3 from the SCR into nitrogen and water vapor using a flow-through substrate that can use various oxidation catalysts. The NH3 delivery systems can also be of various approaches that are in the literature. The concept of a DOC_2 downstream of a CPF before the urea injector should also enhance the NO_x conversion efficiency of the system.

The future EPA and CARB ultra low NO_x standards necessitates a significant decrease in tailpipe NO_x for both in use and certification cycles. These new standards also require better in-use performance and consider the impact of long-term aging. In order to meet all these requirements substantial improvements in system performance and more robust control system similar to the ones presented in this work are required.

Contact Information

Venkata Rajesh Chundru
Michigan Technological University
Houghton, MI US 49931
Phone: +19062818993
vrchundr@mtu.edu

Definitions/Abbreviations

1D - 1 Dimensional
2D - 2 Dimensional
AMOX - Ammonia oxidation catalyst
ANR - Ammonia-to-NO_x ratio
ASC - Ammonia slip catalyst
CARB - California Air Resources Board
CO - Carbon monoxide
CO_2 - Carbon dioxide
CPF - Catalyzed particulate filter
CSF - Catalyzed soot filter
CuO - Cupric oxide
Cu-Ze - Copper zeolite
$C_{12}H_{24}$ - Dodecane
DOC - Diesel oxidation catalyst
DPF - Diesel particulate filter
EPA - Environmental Protection Agency
FTP - Federal Test Procedure
H_2O - Water
MB - Mini burner
NH_3 - Ammonia
NO_2 - Nitrogen dioxide
NO_x - Oxides of nitrogen
N_2O - Nitrous oxide
O_2 - Oxygen
PM - Particulate matter
PNA - Passive NO_x adsorber

SCR - Selective catalytic reduction
SCRF® - Johnson Matthey SCR-F
SCR-A - SCR brick
SCR-B - SCR brick with AMOX coating at the end
SCR-F - SCR catalyst on a DPF
WHTC - World Harmonized Transient Cycle
a - Channel width
A_g - Geometric surface area
$C_{1,l}$ - Inlet channel concentration of species
$C_{1s,l}$ - Inlet channel-wall boundary concentration
$C_{2,l}$ - Concentration in the outlet channel
$C_{2s,l}$ - Concentration at outlet channel-wall boundary
$C_{f,l}$ - Concentration of species l in wall and PM cake
C_c - Specific heat of cake
C_g^n - Concentration of species in gas phase at time n
c_p - Constant pressure specific heat of exhaust gas
c_v - Constant volume specific heat of exhaust gas
C_w - Specific heat of substrate wall
D_l - Diffusion rate
K_1 - Mass transfer coefficient in inlet channel
K_2 - Mass transfer coefficient in outlet channel
l - Species index
m - Index for reactions
$\dot{m}_{1,in}$ - Mass flow rate inlet channel
$\dot{m}_{2,in}$ - Mass flow rate in outlet channel
$\dot{Q}_1$ - Convection heat transfer rate in inlet channel
$\dot{Q}_2$ - Convection heat transfer rate in outlet channel
$\dot{Q}_f$ - Convection heat transfer rate in filter
$R_{ads,1}$ - Adsorption reaction rate at site 1
$R_{ads,2}$ - Adsorption reaction at site 2
$R_{des,1}$ - Desorption reaction rate at site 2
$R_{des,2}$ - Desorption reaction at site 2
R_{fst} - Fast SCR reaction rate
R_m - Reaction rate
R_{oxid} - NH_3 oxidation reaction rate
R_{slo} - Slow SCR reaction rate
R_{std} - Standard SCR reaction rate
T_1 - Temperature in the inlet channel
T_2 - Temperature in the outlet channel
V_1 - Volume of inlet channel
v_1 - Exhaust gas velocity in inlet channel
V_2 - Volume of outlet channel
v_2 - Exhaust gas velocity in the outlet channel
V_f - Volume of filter
v_f - Exhaust gas velocity in the substrate wall
Ω_1 - Maximum storage capacity of storage site 1
Ω_2 - Maximum storage at storage site 2
β_j - Mass transfer coefficient
θ_1 - Coverage fraction of storage site 1
θ_2 - Coverage fraction at storage site 2
$\xi_b m$ - Stoichiometric coefficient
ρ_c - Density of PM cake
ρ_g - Density of exhaust gas
ρ_w - Density of substrate wall
ϵ - Void fraction

References

1. "California Air Resources Board Staff Current Assessment of the Technical Feasibility of Lower NOx Standards and Associated Test Procedures for 2022 and Subsequent Model Year Medium-Duty and Heavy-Duty Diesel Engines," CARB staff white paper, 2019.
2. Surenahalli, H.S., "Dynamic Model Based State Estimation in a Heavy-Duty Diesel Aftertreatment System for Onboard Diagnostics and Controls," Dissertation, Michigan Technological University, 2013.
3. Chundru, V.R., Mahadevan, B.S., Johnson, J.H., Parker, G.G., and Shahbakhti, M., "Development of a 2D Model of a SCR Catalyst on a DPF," *Journal of Emission Control Science and Technology*, 2019, https://doi.org/10.1007/s40825-019099115-4.
4. Song, X., "A SCR Model Based on Reactor and Engine Experimental Studies for a Cu-zeolite Catalyst," PhD Dissertation, Michigan Technological University, 2013.
5. Chundru, V., Parker, G., and Johnson, J., "The Effect of NO_2/NO_x Ratio on the Performance of a SCR Downstream of a SCR Catalyst on a DPF," *SAE Int. J. Fuels Lubr.* 12(2):121-141, 2019. https://doi.org/10.4271/04-12-02-0008.
6. Kadam, V., "An Experimental Investigation of the Effect of Temperature and Space Velocity on the Performance of a Cu-Zeolite Flow-through SCR and a SCR Catalyst on a DPF with and without PM Loading," M.S. thesis, Michigan Technological University, 2016.
7. Gustafson, E.A., "An Experimental Investigation into NO_2 Assisted Passive Oxidation with and without Urea Dosing and Active Regeneration of Particulate Matter for a SCR Catalyst on a DPF," M.S. thesis., Michigan Technological University, 2016.
8. Sharma, S., "The Emission and Particulate Matter Oxidation Performance of a SCR Catalyst on a Diesel Particulate Filter with a Downstream SCR," M.S. Report, Michigan Technological University, 2017.
9. Song, X., Johnson, J.H., and Naber, J.D., "A Review of the Literature of Selective Catalytic Reduction Catalysts Integrated into Diesel Particulate Filters," *International Journal of Engine Research* 16(6):738-749, 2015.
10. Park, S.-Y., Narayanaswamy, K., Schmieg, S.J., and Rutland, C.J., "A Model Development for Evaluating Soot-NOx Interactions in a Blended 2-Way Diesel Particulate Filter/

Selective Catalytic Reduction," *Industrial & Engineering Chemistry Research* 51(48):15582-15592, 2012.

11. Park, S.Y., Rutland, C.J., Narayanaswamy, K., Schmieg, S.J. et al., "Development and Validation of a Model for Wall-Flow Type Selective Catalytic Reduction System," *Proceedings of the Institution of Mechanical Engineers, Part D: Journal of Automobile Engineering* 225(12):1641-1659, 2011.
12. Yang, Y., Cho, G., and Rutland, C., "Model Based Study of DeNOx Characteristics for Integrated DPF/SCR System over Cu-Zeolite," SAE Technical Paper 2015-01-1060, 2015, https://doi.org/10.4271/2015-01-1060.
13. Colombo, M., Koltsakis, G., and Koutoufaris, I., "A Modeling Study of Soot and de-NOx Reaction Phenomena in SCRF Systems," SAE Technical Paper 2011-37-0031, 2011, https://doi.org/10.4271/2011-37-0031.
14. López-De Jesús, Y.M., Chigada, P.I., Watling, T.C., Arulraj, K. et al., "NOx and PM Reduction from Diesel Exhaust Using Vanadia SCRF®," *SAE Int. J. Engines* 9(2):1247-1257, 2016, https://doi.org/10.4271/2016-01-0914.
15. Dosda, S., Berthout, D., Mauviot, G., and Nogre, A., "Modeling of a DOC SCR-F SCR Exhaust Line for Design Optimization Taking into Account Performance Degradation due to Hydrothermal Aging," *SAE Int. J. Fuels Lubr.* 9(3):621-632, 2016, https://doi.org/10.4271/2016-01-2281.
16. Tan, J., Solbrig, C., and Schmieg, S.J., "The Development of Advanced 2-Way SCR/DPF Systems to Meet Future Heavy-Duty Diesel Emissions," SAE Technical Paper 2011-01-1140, 2011, https://doi.org/10.4271/2011-01-1140.
17. Tronconi, E., Nova, I., Marchitti, F., Koltsakis, G. et al., "Interaction of NOx Reduction and Soot Oxidation in a DPF with Cu-zeolite SCR Coating," *Emission Control Science and Technology* 1(2):134-151, 2015.
18. Sharp, C., Webb, C.C., Neely, G., Carter, M. et al., "Achieving Ultra Low NO X Emissions Levels with a 2017 Heavy-Duty On-Highway TC Diesel Engine and an Advanced Technology Emissions System-NOx Management Strategies," *SAE Int. J. Engines* 10(4):1736-1748, 2017, https://doi.org/10.4271/2017-01-0958.
19. Sharp, C., Webb, C.C., Neely, G., Carter, M. et al., "Achieving Ultra Low NO X Emissions Levels with a 2017 Heavy-Duty On-Highway TC Diesel Engine and an Advanced Technology Emissions System-Thermal Management Strategies," *SAE Int. J. Engines* 10:1697-1712, 2017, https://doi.org/10.4271/2017-01-0954.
20. Sharp, C., Webb, C.C., Yoon, S., Carter, M., and Henry, C., "Achieving Ultra Low NOX Emissions Levels with a 2017 Heavy-Duty On-Highway TC Diesel Engine-Comparison of Advanced Technology Approaches," *SAE Int. J. Engines* 10:1722-1735, 2017, https://doi.org/2017-01-0956.
21. Strots, V., Kishi, A., Adelberg, S., and Krämer, L., "Application of Integrated SCR/DPF Systems in Commercial Vehicles," JSAE Annual Congress, 454, 2014.
22. Georgiadis, E., Kudo, T., Herrmann, O., Uchiyama, K., and Hagen, J., "Real Driving Emission Efficiency Potential of SDPF Systems without an Ammonia Slip Catalyst," SAE Technical Paper 2017-01-0913, 2017, https://doi.org/10.4271/2017-01-0913.
23. Hruby, E., Huang, S., Duddukuri, R., and Dou, D., "NOx Performance Degradation of Aftertreatment Architectures Containing DOC with SCR on Filter or Uncatalyzed DPF Downstream of DEF Injection," SAE Technical Paper 2019-01-0740, 2019, https://doi.org/10.4271/2019-01-0740.
24. Dahodwala, M., Joshi, S., Koehler, E., Franke, M. et al., "Strategies for Meeting Phase 2 GHG and Ultra-Low NOx Emission Standards for Heavy-Duty Diesel Engines," *SAE Int. J. Engines* 11(6):1109-1122, 2018, https://doi.org/10.4271/2018-01-1429.
25. Sanchez, J., "EPA's Cleaner Trucks Initiative," presentation in *Symposium on Technologies to Meet Ultra-Low NOx Systems*, University of Wisconsin Madison, 2019.
26. Robertson, W., "Directions and Opportunities for Realizing Heavy Duty Emissions Reductions In-Use," presentation in *Symposium on Technologies to Meet Ultra-Low NOx Systems*, University of Wisconsin Madison, 2019.
27. Stanton, D., "The Future of Highly Efficient, Clean IC Engine to Meet Global Emissions Requirement," presentation in *Symposium on Technologies to Meet Ultra-Low NOx Systems*, University of Wisconsin Madison, 2019.
28. Dunnuck, D., "Perspective on Ultra-Low NOx Emissions, Technical Paths and Challenges," presentation in *Symposium on Technologies to Meet Ultra-Low NOx Systems*, University of Wisconsin Madison, 2019.
29. Miwa, J., "Update on CARB Low NOx Program," presentation in *Symposium on Technologies to Meet Ultra-Low NOx Systems*, University of Wisconsin Madison, 2019.
30. Patchett, J.A., Dettling, J.C., and Prybylski, E.A., "Catalyzed SCR Filter and Emission Treatment System," U.S. Patent No. US8,899,023 B2. Washington, DC: U.S. Patent and Trademark Office, December 2, 2014.
31. Patchett, J.A., Dettling, J.C., and Przybylski, E.A., "Catalyzed SCR Filter and Emission Treatment System," U.S. Patent No. US9,039,982 B2. Washington, DC: U.S. Patent and Trademark Office, May 26, 2015.
32. Patchett, J.A., Dettling, J.C., and Pryzybylski, E.A., "Catalyzed SCR Filter and Emission Treatment System," U.S. Patent No. US9,039,983. Washington, DC: U.S. Patent and Trademark Office, May 26, 2015
33. Patchett, J.A., Dettling, J.C., and Pryzybylski, E.A., "Catalyzed SCR Filter and Emission Treatment System," U.S. Patent No. US9,039,984. Washington, DC: U.S. Patent and Trademark Office, May 26, 2015.
34. Patchett, J.A., Dettling, J.C., and Pryzybylski, E.A., "Catalyzed SCR Filter and Emission Treatment System," U.S. Patent No. US9,040,006. Washington, DC: U.S. Patent and Trademark Office, May 26, 2015.
35. Patchett, J.A., Dettling, J.C., and Pryzybylski, E.A., "Catalyzed SCR Filter and Emission Treatment System," U.S. Patent No. US9,121,327. Washington, DC: U.S. Patent and Trademark Office, September 1, 2015.
36. Patchett, J.A., Dettling, J.C., and Pryzybylski, E.A., "Catalyzed SCR Filter and Emission Treatment System," U.S. Patent No. US9,144,795 B2. Washington, DC: U.S. Patent and Trademark Office, September 29, 2015.

37. Patchett, J.A., Dettling, J.C., and Pryzybylski, E.A., "Catalyzed SCR Filter and Emission Treatment System," U.S. Patent No. US9,517,455 B2. Washington, DC: U.S. Patent and Trademark Office, December 13, 2016.

38. Patchett, J.A., Dettling, J.C., and Pryzybylski, E.A., "Catalyzed SCR Filter and Emission Treatment System," U.S. Patent No. US9,517,456 B2. Washington, DC: U.S. Patent and Trademark Office, December 13, 2016.

39. Patchett, J.A., Dettling, J.C., and Prybylski, E.A., "Methods for Disposing SCR Composition on a wall Flow Monolith," U.S. Patent No. US9,757,717 B2. Washington, DC: U.S. Patent and Trademark Office, September 12, 2017.

40. Song, X., Naber, J., and Johnson, J.H., "Nonuniformity and NO_2/NO_x Ratio Effects on the SCR Performance under Transient Engine Conditions," SAE Technical Paper 2014-01-1556, 2014, https://doi.org/10.4271/2014-01-1556.

41. Chundru, V., "Development of a 2D SCR Catalyst on a Diesel Particulate Filter Model for Design and Control Applications to a Ultra Low NOx Aftertreatment System," PhD Dissertation, Michigan Technological University, 2019.

42. Su, C., Brault, J., Munnannur, A., Liu, Z. et al., "Model-Based Approaches in Developing an Advanced Aftertreatment System: An Overview," *SAE Int. J. Adv. & Curr. Prac. in Mobility* 1(1):201-214, 2019, https://doi.org/10.4271/2019-01-0026.

Appendix A: Model Results

Figures 15, 16, A.1 and A.2 show the performance of the SCR-F + DOC_2 + SCR system for the experimental data from Table 2. These experiments cover a wide range of exhaust temperature and flow rate conditions along with inlet NO_2/NO_x ratio and NO_x concentrations at the inlet of the SCR-F.

Test 1. Inlet T = 203°C, NO = 443 ppm, NO_2 = 182 ppm, NO_x = 625 ppm, Flow Rate = 5.2 kg/min.
Test A. Inlet T = 267°C, NO = 375 ppm, NO_2 = 215 ppm, NO_x = 590 ppm, Flow Rate = 5.6 kg/min.
Test D - Inlet T = 366°C, NO = 289 ppm, NO_2 = 161 ppm, NO_x = 450 ppm, Flow Rate = 12.5 kg/min
Test E - Inlet T = 342°C, NO = 866 ppm, NO_2 = 584 ppm, NO_x = 1450 ppm, Flow Rate = 7.1 kg/min

FIGURE A.1 NO_x conversion efficiency, ANR_2, PM oxidation rate, SCR-F outlet NO_2 and SCR outlet NH_3 concentration vs ANR_1 at engine condition 1 (SCR-F + DOC_2 + SCR with two urea injectors).

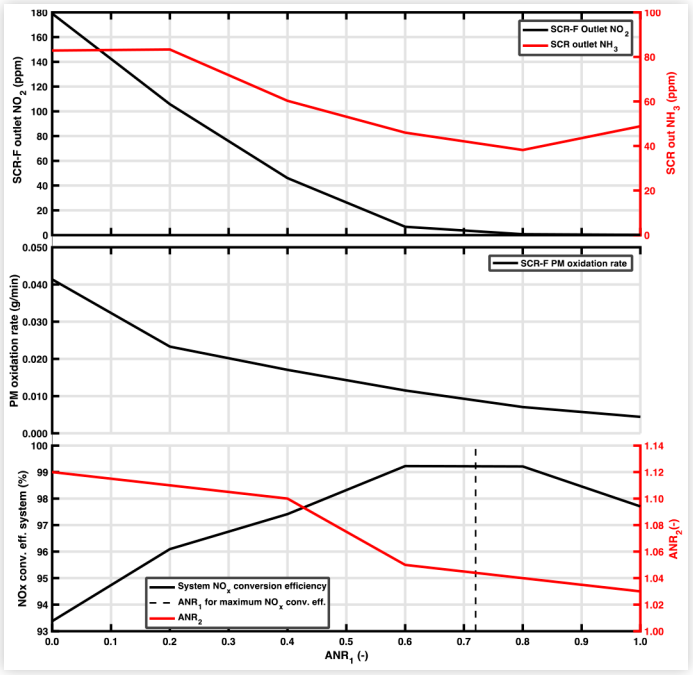

FIGURE A.2 NO_x conversion efficiency, ANR_2 , PM oxidation rate, SCR-F outlet NO_2 and SCR outlet NH_3 concentration vs ANR_1 at engine condition A (SCR-F + DOC_2 + SCR with 2 urea injectors).

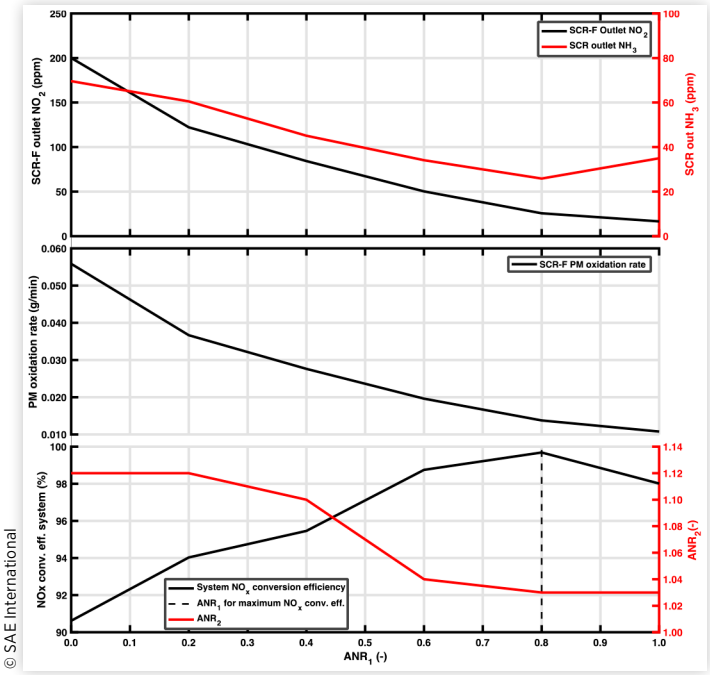

FIGURE A.3 NO_x conversion efficiency, ANR_2, PM oxidation rate, SCR-F outlet NO_2 and SCR outlet NH_3 concentration vs. ANR_1 at engine condition D (SCR-F + DOC_2 + SCR system with two urea injectors).

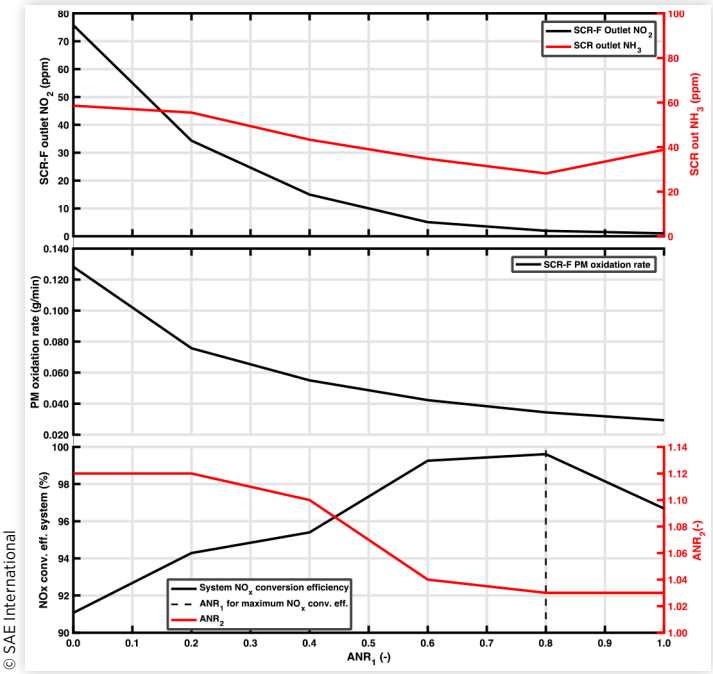

FIGURE A.4 NO_x conversion efficiency, ANR_2 , PM oxidation rate, SCR-F outlet NO_2 and SCR outlet NH_3 concentration vs. ANR_1 at engine condition E (SCR-F + DOC_2 + SCR with two urea injectors).